Computer Assisted Mechanics and Engineering Sciences, 9: 315–340, 2002.

A novel momentum-preserving energy-decaying algorithm for finite-element multibody procedures[1]

Marco Borri, Carlo L. Bottasso and Lorenzo Trainelli
Politecnico di Milano, Dipartimento di Ingegneria Aerospaziale
Via La Masa 34, 20158, Milano, Italy

(Received August 8, 2000)

We present a new methodology for the integration of general non-linear multibody systems within a finite-element framework, with special attention to numerical robustness. The outcome is a non-linearly unconditionally stable algorithm with dissipation properties. This algorithm exactly preserves the total linear and angular momenta of holonomically constrained multibody systems, which implies the satisfaction of Newton's Third law of Action and Reaction. Furthermore, the scheme strictly dissipates the total mechanical energy of the system. This is accomplished by selective damping of the unresolved high-frequency components of the response. We derive the governing equations relying on the 6-D compact representation of motion and we employ a parameterization based on the Cayley transform which ensures geometric invariance of the resulting numerical schemes. We present some numerical tests in order to illustrate the main features of the methodology, and to demonstrate the properties predicted in the analysis.

1. Introduction

The dynamic simulation of flexible multibody systems with general topologies involves the solution of *stiff*, non-linear differential-algebraic equations (DAEs). The causes of numerical stiffness are usually recognized both in the presence of kinematic constraints and in the possible excitation of the spurious high-frequency components that are present in the response as a result of the spatial discretization of deformable bodies (for example, via finite element methods). Stiffness often implies serious numerical difficulties in the solution of the governing equations, resulting in a typical highly oscillatory behavior of the response that can prevent the convergence of the Newton process performed at each time step. This, together with the geometric non-linearities arising from the description of large displacements and finite rotations, clearly poses particular robustness requirements upon the numerical procedures.

Although a significant effort has been made in recent times to devise robust numerical schemes capable of coping with these issues, the great majority of the available algorithms is based only on *linear* notions of stability, giving no warranty of their success in the non-linear regime which characterizes multibody applications. Furthermore, by using classical integrators, distinctive qualitative features of the solution are usually *lost* at the numerical level.

Among these features, the most relevant in this context are the conservation of linear and angular momenta, and of the total mechanical energy. Indeed, unconditional stability in the non-linear regime is strictly associated with discrete conservation laws. For example, energy/momentum algorithms for rigid bodies, geometrically exact beams and shells are presented in [12–14]. However, even if energy conservation ensures unconditional stability, experience has shown that energy preserving integrators can fail due to uncontrolled energy transfers from the low to the high frequency modes. It is important to realize that this is a completely non-physical process, since the higher modes of a finite element model are a pure artifact of the spatial discretization, and bear no resemblance to the behavior of the original system.

[1]This is an extended version of the article presented at the NATO Advanced Research Workshop on the *Computational Aspects of Nonlinear Structural Systems with Large Rigid Body Motion*, Pułtusk, Poland, July 2–7, 2000.

A methodology for overcoming these difficulties was presented in [6, 7, 9, 10] as well as in [1–4] along similar guidelines. The design of a non-linearly stable integrator with control of the unresolved frequencies becomes then a three-step process. First, an energy preserving scheme for unconstrained deformable bodies is obtained. Then, the constraints that model various mechanical joints are introduced. The reaction forces exerted by the joints on the bodies are discretized so as to guarantee the vanishing of the work at the discrete solution level, so that energy preservation can be proved for the whole multibody system. Finally, two coupled energy preserving steps are combined to yield an energy decaying scheme, that combines non-linear unconditional stability from the bound on the total energy together with high frequency numerical damping. Ref. [1] discusses the application of these ideas to general 3-D continua, beams, shells, and multibody systems comprised of these elements.

The methodology proposed here represents a further refinement of the framework just described. We design a non-linearly unconditionally stable energy decaying scheme that achieves an additional invariant property: the *conservation of linear momentum and angular momentum with respect to any fixed pole.* This is guaranteed by a time discretization of the inertial terms that naturally preserves momenta of unconstrained bodies, together with an expression for the reaction forces exerted by a mechanical joint on two connected bodies that ensures they are equal and opposite (Newton's Third Law). In fact, it should be remarked that Newton's Third Law is usually not satisfied by other energy preserving or decaying algorithms. Such a result is obtained by employing the Cayley parameterization of motion, a novel 'global' parameterization technique recently proposed in [5]. We briefly present the 6-D representation and parameterization of motion for the cases of rigid bodies and geometrically exact beams. Next, we formulate a second order, non-linearly unconditionally stable momentum and energy preserving scheme, that is then used for constructing the momentum preserving, energy decaying scheme. Some numerical applications complete the present work, illustrating the basic features of the proposed algorithm.

2. Governing equations

The motion of rigid and deformable bodies such as beams and shells can be conveniently described by considering the rotation field together with the displacement field, and then by operating on them as a single quantity. This leads to the *6-D compact representation of motion.* Central roles in this representation are played by the concept of configuration as the union of both the position and orientation information, as well as the notion of reduction to the base pole for kinematic and dynamic quantities. Furthermore, the 6-D representation naturally calls for the development of a 'global', or intrinsically coupled, parameterization technique for frame motion termed *Cayley's parameterization.* This employs a minimal number of coordinates, i.e. 6 scalars, accounting for both position and orientation. We remark that any numerical scheme based on the base pole formulation is geometrically invariant, i.e. it correctly represents changes of placement of reference entities (a point and a triad of body attached unit vectors on a rigid body, a reference curve and an associated field of unit triads along a beam, a reference surface and an associated field of directors for a shell), as pointed out in [2, 8].

2.1. 6-D compact kinematics

2.1.1. Frame kinematics

The basic notion for the 6-D representation of motion is that of a *frame.* This is given by the ordered set composed by a *pole*, i.e. a placement in the 3-D Euclidean space $\mathcal{E}^3$, and a triad of mutually orthogonal unit vectors of the translation space $\mathbb{E}^3$. These vectors originate at the pole. We consider two such frames: the *base frame* $(\mathbf{o}, \{\mathbf{i}_k\}_{k=1,2,3})$ and the *moving frame* $(\mathbf{x}, \{\mathbf{e}_k\}_{k=1,2,3})$. The latter is used to describe the configuration of rigid as well as deformable bodies with respect to the former,

which holds fixed at all times. In fact, the configuration of the moving frame with respect to the base frame may be specified by the pair $(\mathbf{u}, \boldsymbol{\alpha})$. Vector $\mathbf{u} \in \mathbb{E}^3$ is the frame position vector, while tensor $\boldsymbol{\alpha} \in \mathrm{SO}(\mathbb{E}^3)$ is the frame orientation tensor. They are defined as

$$\mathbf{u} := \mathbf{x} - \mathbf{o}, \qquad \boldsymbol{\alpha} := \mathbf{e}_k \otimes \mathbf{i}_k \,. \tag{1}$$

The set $\mathrm{SO}(\mathbb{E}^3)$ is the group of the special orthogonal tensors of $\mathrm{Lin}(\mathbb{E}^3)$, or *rotation group*. The tensors belonging to $\mathrm{SO}(\mathbb{E}^3)$ are unimodular, $\det(\boldsymbol{\alpha}) = +1$, and orthogonal, $\boldsymbol{\alpha}^{-1} = \boldsymbol{\alpha}^T$.

In the 6-D compact representation we work with the *frame configuration tensor* $\mathbf{C} \in \mathrm{SR}(\mathbb{K}^6)$ as a convenient quantity in a one-to-one correspondence to the configuration pair $(\mathbf{u}, \boldsymbol{\alpha})$. This 6-D tensor is defined by the following matricial expression,

$$\mathbf{C} := \begin{bmatrix} \boldsymbol{\alpha} & \mathbf{u} \times \boldsymbol{\alpha} \\ \mathbf{O} & \boldsymbol{\alpha} \end{bmatrix}. \tag{2}$$

The set $\mathrm{SR}(\mathbb{K}^6)$ is termed the group of the special rigid displacement tensors of $\mathrm{Lin}(\mathbb{K}^6)$. It is clearly isomorphic to the *Euclidean group*, i.e. the configuration space $\mathbb{E}^3 \times \mathrm{SO}(\mathbb{E}^3)$ of the moving frame with respect to the base frame. Tensors belonging to $\mathrm{SR}(\mathbb{K}^6)$ are unimodular, $\det(\mathbf{C}) = +1$. Taking the time derivative of tensor $\mathbf{C}$ yields the expressions

$$\dot{\mathbf{C}} = \mathbf{w}\times\mathbf{C} = \mathbf{C}\,\overline{\mathbf{w}}\times, \tag{3}$$

where superposed dots denote differentiation with respect to time t. The 6-D vectors $\mathbf{w} := (\mathbf{v}; \boldsymbol{\omega}) \in \mathbb{K}^6$ and $\overline{\mathbf{w}} = (\overline{\mathbf{v}}; \overline{\boldsymbol{\omega}}) \in \mathbb{K}^6$ are the *frame base pole generalized velocity* and the *frame convected generalized velocity*, respectively.[2] The *kinematic space* $\mathbb{K}^6$ is simply given by the direct sum of two copies of $\mathbb{E}^3$, $\mathbb{K}^6 := \mathbb{E}^3 \oplus \mathbb{E}^3$.

The 3-D vector components of vector $\mathbf{w}$ are the frame base pole linear velocity $\mathbf{v} \in \mathbb{E}^3$ and the frame angular velocity $\boldsymbol{\omega} \in \mathbb{E}^3$, respectively defined as

$$\mathbf{v} := \dot{\mathbf{u}} + \mathbf{u} \times \boldsymbol{\omega}, \qquad \boldsymbol{\omega} := \mathrm{axial}_\times(\dot{\boldsymbol{\alpha}}\,\boldsymbol{\alpha}^{-1}), \tag{4}$$

where $\mathrm{axial}_\times : \mathrm{so}(\mathbb{E}^3) \longrightarrow \mathbb{E}^3$ performs the extraction of the axial vector $\bullet$ from a skew-symmetric tensor $(\bullet\times)$, while the 3-D components of vector $\overline{\mathbf{w}}$ are their convected images $\overline{\mathbf{v}}$ and $\overline{\boldsymbol{\omega}}$, respectively defined as

$$\overline{\mathbf{v}} := \boldsymbol{\alpha}^{-1}\dot{\mathbf{u}}, \qquad \overline{\boldsymbol{\omega}} := \mathrm{axial}_\times(\boldsymbol{\alpha}^{-1}\dot{\boldsymbol{\alpha}}). \tag{5}$$

Note that, while for the rotational rates the relation between 'spatial' and convected angular velocities implies only the rotation from the moving axes to the base axes, i.e.

$$\boldsymbol{\omega} = \boldsymbol{\alpha}\,\overline{\boldsymbol{\omega}}, \tag{6}$$

for the translational rates the relation between the 'base pole' and convected linear velocities implies also the transport from the moving pole to the base pole, i.e.

$$\mathbf{v} = \boldsymbol{\alpha}\,\overline{\mathbf{v}} + \mathbf{u} \times (\boldsymbol{\alpha}\,\overline{\boldsymbol{\omega}}). \tag{7}$$

The base pole linear velocity has a remarkable significance. In fact, for a material frame it is independent of the choice of the frame pole, and therefore it represents a global measure, analogously to the angular velocity. On the other hand, in terms of generalized rates, the relation between base pole and convected generalized velocities keeps the formal simplicity of the rotational case, as it reads

$$\mathbf{w} = \mathbf{C}\,\overline{\mathbf{w}}. \tag{8}$$

[2]Here, and in the following, we make use of the semicolon in the representation of 6-D vectors as a short notation for the more cumbersome expressions $\mathbf{w} := (\mathbf{v}^T, \boldsymbol{\omega}^T)^T$ and $\overline{\mathbf{w}} = (\overline{\mathbf{v}}^T, \overline{\boldsymbol{\omega}}^T)^T$.

Note that Eq. (3) represents the 6-D version of the classical

$$\dot{\boldsymbol{\alpha}} = \boldsymbol{\omega} \times \boldsymbol{\alpha} = \boldsymbol{\alpha}\,\overline{\boldsymbol{\omega}} \times . \tag{9}$$

In particular, they share an identical structure, except for the substitution of the cross product operation $\times$ with the *North-East generalized cross product* operation $\nearrow$, that represents the commutator for $\mathbb{K}^6$, i.e. a bilinear, skew-symmetric operation that verifies the Jacobi identity. This extension to 6-D space of the standard commutator for $\mathbb{E}^3$ is defined by the following matricial expressions,

$$\mathbf{w}\nearrow = \begin{bmatrix} \boldsymbol{\omega}\times & \mathbf{v}\times \\ \mathbf{O} & \boldsymbol{\omega}\times \end{bmatrix}, \qquad \overline{\mathbf{w}}\nearrow = \begin{bmatrix} \overline{\boldsymbol{\omega}}\times & \overline{\mathbf{v}}\times \\ \mathbf{O} & \overline{\boldsymbol{\omega}}\times \end{bmatrix}. \tag{10}$$

In analogy to Eqs. $(4)_2$, $(5)_2$ we write

$$\mathbf{w} := \mathrm{axial}_{\nearrow}(\dot{\mathbf{C}}\,\mathbf{C}^{-1}), \qquad \overline{\mathbf{w}} := \mathrm{axial}_{\nearrow}(\mathbf{C}^{-1}\dot{\mathbf{C}}), \tag{11}$$

where $\mathrm{axial}_{\nearrow} : \mathrm{sr}(\mathbb{K}^6) \longrightarrow \mathbb{K}^6$ extracts the 6-D vector $\bullet$ from the north-east cross product tensor $(\bullet\nearrow)$. Since the set of all skew-symmetric 3-D tensors forming the Lie algebra of $\mathrm{SO}(\mathbb{E}^3)$ are denoted by $\mathrm{so}(\mathbb{E}^3)$, we denote by the symbol $\mathrm{sr}(\mathbb{K}^6)$ the set of all 6-D tensors of the form $(\bullet\nearrow)$ that compose the Lie algebra of $\mathrm{SR}(\mathbb{K}^6)$.

It should be easily seen that the introduction of the configuration tensor and of the generalized velocity leads to a unified treatment of both position and orientation and their respective time-rates, for the general motion of a frame (which coincides with a general *rigid* motion). We remark that the employed formalism shares an almost identical structure and appearance with the one that is used in the case of the reduced problem of pure rotational motion.

2.1.2. Relative frame kinematics

Consider two moving frames denoted by the subscripts A and B. Their configuration with respect to the base frame is represented by the configuration pairs $(\mathbf{u}_A\,,\,\boldsymbol{\alpha}_A)$ and $(\mathbf{u}_B\,,\,\boldsymbol{\alpha}_B)$, or equivalently by the configuration tensors $\mathbf{C}_A$ and $\mathbf{C}_B$, as smooth functions of time t.

We consider the relative configuration of frame B with respect to A as specified by means of the *convected relative displacement tensor* $\overline{\mathbf{D}} \in \mathrm{SR}(\mathbb{K}^6)$ defined as

$$\overline{\mathbf{D}} := \mathbf{C}_A^{-1}\mathbf{C}_B\,. \tag{12}$$

The matricial expression of the convected relative displacement tensor is given by

$$\overline{\mathbf{D}} = \begin{bmatrix} \overline{\mathbf{R}} & (\boldsymbol{\alpha}_A^{-1}\Delta\mathbf{u}) \times \overline{\mathbf{R}} \\ \mathbf{O} & \overline{\mathbf{R}} \end{bmatrix}, \tag{13}$$

where $\Delta\mathbf{u} \in \mathbb{E}^3$ and $\overline{\mathbf{R}} \in \mathrm{SO}(\mathbb{E}^3)$ are the relative displacement vector and the convected relative rotation vector, respectively, defined as

$$\Delta\mathbf{u} := \mathbf{u}_B - \mathbf{u}_A\,, \qquad \overline{\mathbf{R}} := \boldsymbol{\alpha}_A^{-1}\boldsymbol{\alpha}_B\,. \tag{14}$$

Let us define the scalar components $\{\overline{d}_{Ak} := \mathbf{e}_{Ak} \cdot \Delta\mathbf{u}\}_{k=1,2,3}$ of the displacement vector with respect to the body A triad $\{\mathbf{e}_{Ak}\}_{k=1,2,3}$ for later convenience. The scalar components $\{\overline{R}_{hk} := \mathbf{i}_h \cdot \overline{\mathbf{R}}\,\mathbf{i}_k\}_{h,k=1,2,3}$ of the convected rotation tensor $\overline{\mathbf{R}}$ with respect to the base triad $\{\mathbf{i}_k\}_{k=1,2,3}$ form the *direction cosine* matrix of frame B with respect to frame A,

$$\overline{\mathbf{R}} = (\mathbf{e}_{Ah} \cdot \mathbf{e}_{Bk})\,\mathbf{i}_h \otimes \mathbf{i}_k\,. \tag{15}$$

Note that the convected displacement tensor $\overline{\mathbf{D}}$ is a constant-in-time quantity whenever the two frames are rigidly connected, that is, whenever they move as parts of a single rigid system. Indeed, in

such a case both the displacement vector and the direction cosines are constant-in-time quantities. If we look at the time derivative of tensor $\overline{\mathbf{D}}$,

$$\dot{\overline{\mathbf{D}}} = (\mathbf{C}_A^{-1}\Delta\mathbf{w})\times\overline{\mathbf{D}}, \tag{16}$$

we find that the 6-D vector characterizing this time-rate is the 'A-convected' image of the *relative generalized velocity* $\Delta\mathbf{w} \in \mathbb{K}^6$, defined as

$$\Delta\mathbf{w} := \mathbf{w}_B - \mathbf{w}_A\,. \tag{17}$$

The above definition identifies a *unique* relative generalized velocity for any two frames rigidly connected to frames A and B. Such property relies on the notion of reduction to the base pole and is clearly lost when one assumes as measure of relative velocity a quantity based on the local linear velocities $\dot{\mathbf{u}}_A$ and $\dot{\mathbf{u}}_B$ of the two frames, instead of their base pole counterparts $\mathbf{v}_A$ and $\mathbf{v}_B$. Furthermore, it is apparent from Eq. (16) that the relative generalized velocity $\Delta\mathbf{w}$ vanishes whenever frames A and B move as if they were rigidly connected.

2.1.3. Constraints between two frames

The mechanical constraints between the various parts of a flexible multibody system can be described as suitable combinations of relatively simple constraints between frame pairs. In particular, *holonomic constraints* impose limitations upon their relative configuration, and hence upon their relative generalized velocities. In fact, any bilateral holonomic constraint between frames A and B may be expressed by a configuration-level equation such as

$$\boldsymbol{\phi}(\overline{\mathbf{D}}, t) = \mathbf{0}. \tag{18}$$

Differentiation of the preceding equation with respect to time leads to the velocity-level equation

$$\mathbf{A}^T\Delta\mathbf{w} + \mathbf{a} = \mathbf{0}. \tag{19}$$

Tensor $\mathbf{A} : \mathbb{R}^K \longrightarrow \mathbb{K}^6$, where the integer $0 < K \leq 6$ is the number of constrained degrees of freedom, is termed the *base pole constraint tensor* and is related to the partial derivative of the constraint function $\boldsymbol{\phi}$ with respect to the convected displacement tensor $\overline{\mathbf{D}}$. Vector $\mathbf{a} \in \mathbb{R}^K$ is termed the *constraint velocity*, since it is simply the partial derivative of the constraint function $\boldsymbol{\phi}$ with respect to time t. Clearly, when the constraint is *scleronomic*, or time-independent, the constraint velocity $\mathbf{a}$ vanishes identically.

Two examples of holonomic constraints of common use in multibody systems are provided in the following to clarify these concepts. We refer to scleronomic constraints for the sake of simplicity.

Consider first a *prismatic joint* $\mathcal{J}_\mathcal{P}$, which prescribes that frame B can only translate with respect to frame A along the direction defined by the unit vector $\mathbf{j}_\mathcal{P}$, fixed in both frames. The two frames are considered initially coincident and their poles placed at any point along the joint axis $\mathbf{j}_\mathcal{P}$. The constraint states that the linear displacement between the frames is parallel to $\mathbf{j}_\mathcal{P}$ and that no relative rotation is allowed,

$$\mathbf{j}_\mathcal{P} \times \Delta\mathbf{u} = \mathbf{0}, \qquad \overline{\mathbf{R}} = \mathbf{I}. \tag{20}$$

The parametric equation for the prismatic joint reads

$$\Delta\mathbf{u} = \rho\,\mathbf{j}_\mathcal{P}\,, \tag{21}$$

where ρ, the scalar relative translation, is the only unconstrained degree of freedom ($K_\mathcal{P} = 5$). If we assume that the $\mathbf{e}_3$ axis of both frames is initially (and hence at any time) aligned with the $\mathbf{j}_\mathcal{P}$ axis of the joint, we may write the constraint function and tensor as

$$\boldsymbol{\phi}_\mathcal{P} = \left[\ \overline{d}_{A1},\ \overline{d}_{A2},\ \overline{R}_{12},\ \overline{R}_{23},\ \overline{R}_{31}\ \right]^T, \qquad \mathbf{A}_\mathcal{P} = \begin{bmatrix} \mathbf{e}_{A1} & \mathbf{e}_{A2} & \mathbf{O} \\ \mathbf{0} & \mathbf{0} & \mathbf{I} \end{bmatrix}. \tag{22}$$

Consider now a *revolute joint* $\mathcal{J}_\mathcal{R}$, which prescribes that frame B can only rotate with respect to frame A about the direction defined by the unit vector $\mathbf{j}_\mathcal{R}$, fixed in both frames. The two frames are considered initially coincident and their poles placed at any point along the joint axis $\mathbf{j}_\mathcal{R}$. The constraint states that no linear displacement between the frames is allowed and that the relative rotation must occur about $\mathbf{j}_\mathcal{R}$,

$$\Delta\mathbf{u} = \mathbf{0}, \qquad (\overline{\mathbf{R}} - \mathbf{I})\,\bar{\mathbf{j}}_\mathcal{R} = \mathbf{0}, \tag{23}$$

where $\bar{\mathbf{j}}_\mathcal{R} := \boldsymbol{\alpha}_A^{-1}\mathbf{j}_\mathcal{R} \equiv \boldsymbol{\alpha}_B^{-1}\mathbf{j}_\mathcal{R}$. The parametric equation for the revolute joint reads

$$\overline{\mathbf{R}} = \mathbf{I} + \sin\varphi\,(\bar{\mathbf{j}}_\mathcal{R}\times) + (1-\cos\varphi)\,(\bar{\mathbf{j}}_\mathcal{R}\times)^2, \tag{24}$$

where φ, the scalar relative rotation, is the only unconstrained degree of freedom ($K_\mathcal{R} = 5$). If we assume that the $\mathbf{e}_3$ axis of both frames is initially (and hence at any time) aligned with the $\mathbf{j}_\mathcal{R}$ axis of the joint, we may write the constraint function and tensor as

$$\boldsymbol{\phi}_\mathcal{R} = \left[\ \bar{d}_{A1},\ \bar{d}_{A2},\ \bar{d}_{A3},\ \overline{R}_{12},\ \overline{R}_{23}\ \right]^T, \qquad \mathbf{A}_\mathcal{R} = \begin{bmatrix} \mathbf{I} & \mathbf{0} & \mathbf{0} \\ \mathbf{u}_B\times & \mathbf{e}_{A1} & \mathbf{e}_{A2} \end{bmatrix}. \tag{25}$$

The formulae for the other lower pairs can be easily obtained in a similar way.

2.2. 6-D compact representation of dynamics

2.2.1. Rigid body dynamics

In the case of a rigid body, a single moving frame is sufficient to describe the whole configuration of body $\mathcal{B}$. We associate inertial properties to the moving frame, represented by a constant-in-time *convected generalized inertia tensor* $\overline{\mathbf{M}}$ defined as

$$\overline{\mathbf{M}} := \begin{bmatrix} m\,\mathbf{I} & -\int_\mathcal{B}(\mathbf{y}-\mathbf{x})\times \mathrm{d}m_\mathbf{y} \\ +\int_\mathcal{B}(\mathbf{y}-\mathbf{x})\times \mathrm{d}m_\mathbf{y} & -\int_\mathcal{B}(\mathbf{y}-\mathbf{x})\times(\mathbf{y}-\mathbf{x})\times \mathrm{d}m_\mathbf{y} \end{bmatrix}, \tag{26}$$

where m denotes the mass and $\mathbf{y} \in \mathcal{E}^3$ the dummy integration point. The lower left block in the previous matrix expression is the static moment of the body with respect to the moving pole $\mathbf{x}$, while the lower right block is the moment of inertia, again referred to $\mathbf{x}$. The generalized inertia tensor is symmetric, and enters the constitutive equation that relates the *base pole generalized kinetic moment* $\mathbf{p} := (\mathbf{l};\mathbf{h}) \in \mathbb{K}^{6*}$ to the convected generalized velocity $\overline{\mathbf{w}}$ as

$$\mathbf{p} := \mathbf{C}^{-T}\overline{\mathbf{M}}\,\overline{\mathbf{w}}. \tag{27}$$

The 3-D vector components of vector $\mathbf{p}$ are the linear momentum $\mathbf{l} \in \mathbb{E}^{3*}$ and the base pole angular momentum $\mathbf{h} \in \mathbb{E}^{3*}$ of body $\mathcal{B}$. The *co-kinematic space* $\mathbb{K}^{6*}$ is simply the dual of $\mathbb{K}^6$, $\mathbb{K}^{6*} := \mathbb{E}^{3*} \oplus \mathbb{E}^{3*}$, $\mathbb{E}^{3*}$ being the dual of $\mathbb{E}^3$.

The *kinetic energy* T may then be written as

$$T := \frac{1}{2}\,\overline{\mathbf{w}}\cdot\overline{\mathbf{M}}\,\overline{\mathbf{w}}. \tag{28}$$

Given a system of forces acting on $\mathcal{B}$, represented by the resultant force $\mathbf{n} \in \mathbb{E}^{3*}$ and the resultant base pole torque $\mathbf{m} \in \mathbb{E}^{3*}$, the *6-D base pole dynamic balance equation* reads

$$\dot{\mathbf{p}} = \mathbf{f}, \tag{29}$$

where $\mathbf{f} := (\mathbf{n};\mathbf{m}) \in \mathbb{K}^{6*}$ is the *resultant base pole generalized force.*

Note that the simplicity of Eq. (29) is the result of the reduction of the torque balance equation $\dot{\mathbf{h}}_\mathbf{x} + \mathbf{v}_\mathbf{x}\times\mathbf{l} = \mathbf{m}_\mathbf{x}$ to the base pole: $\mathbf{h} = \mathbf{m}$, with $\mathbf{h} = \mathbf{h}_\mathbf{x} + \mathbf{u}\times\mathbf{l}$ and $\mathbf{m} = \mathbf{m}_\mathbf{x} + \mathbf{u}\times\mathbf{n}$. This procedure annihilates the term that couples the torque balance with the force balance equation $\dot{\mathbf{l}} = \mathbf{n}$ when one refers to the moving pole $\mathbf{x}$.

2.2.2. *Beam dynamics*

Next, we consider the case of a geometrically exact beam. In this case a smooth one-parameter family of moving frames describes the configuration of beam $\mathcal{B}$. We consider a material abscissa $s \in [0, L]$ as the parameter. The moving pole $\mathbf{x}(s)$ describes then a smooth line in $\mathcal{E}^3$, the beam *axis*. The triad $\{\mathbf{e}_k(s)\}_{k=1,2,3}$ represent the oriented 'cross section' of the beam. The configuration of the beam is then represented by a one-parameter family of configuration tensors $\mathbf{C}(s) \in \mathrm{SR}(\mathbb{K}^6)$, whose s-rate is given by

$$\mathbf{C}' = \boldsymbol{\chi}^{\times}\mathbf{C} = \mathbf{C}\overline{\boldsymbol{\chi}}^{\times}, \tag{30}$$

where $(\bullet)'$ denotes differentiation with respect to the material abscissa s. The 6-D vectors $\boldsymbol{\chi} := (\boldsymbol{\tau}; \boldsymbol{\kappa}) \in \mathbb{K}^6$ and $\overline{\boldsymbol{\chi}} = (\overline{\boldsymbol{\tau}}; \overline{\boldsymbol{\kappa}}) \in \mathbb{K}^6$ are the *frame base pole generalized curvature* and the *frame convected generalized curvature*, respectively.

The 3-D vector components of vector $\boldsymbol{\chi}$ are the axis tangent vector reduced to the base pole $\boldsymbol{\tau} \in \mathbb{E}^3$ and the curvature $\boldsymbol{\kappa} \in \mathbb{E}^3$, respectively defined as

$$\boldsymbol{\tau} := \mathbf{u}' + \mathbf{u} \times \boldsymbol{\kappa}, \qquad \boldsymbol{\kappa} := \mathrm{axial}_{\times}(\boldsymbol{\alpha}' \boldsymbol{\alpha}^{-1}), \tag{31}$$

while the 3-D vector components of $\overline{\boldsymbol{\chi}}$ are their convected images $\overline{\boldsymbol{\tau}} \in \mathbb{E}^3$ and $\overline{\boldsymbol{\kappa}} \in \mathbb{E}^3$, respectively defined as

$$\overline{\boldsymbol{\tau}} := \boldsymbol{\alpha}^{-1}\mathbf{u}', \qquad \overline{\boldsymbol{\kappa}} := \mathrm{axial}_{\times}(\boldsymbol{\alpha}^{-1}\boldsymbol{\alpha}'). \tag{32}$$

Additionally, we impose the constraint $\mathbf{u}' \cdot \mathbf{e}_3 = \overline{\boldsymbol{\tau}} \cdot \mathbf{i}_3 > 0$, $\forall s \in [0, L]$, to preserve the physical consistency of the model.

The beam deformation is described with respect to a *natural* (stress-free) configuration denoted by the subscript $(\bullet)_N$. A convenient strain measure is the *convected generalized strain* $\overline{\boldsymbol{\varepsilon}} \in \mathbb{K}^6$ defined as

$$\overline{\boldsymbol{\varepsilon}} := \overline{\boldsymbol{\chi}} - \overline{\boldsymbol{\chi}}_N \,. \tag{33}$$

This quantity is clearly unaffected by global rigid displacements of the beam. The scalar components with respect to the base axes $\{\mathbf{i}_k\}_{k=1,2,3}$ of the linear 3-D vector of $\overline{\boldsymbol{\varepsilon}}$ represent the local axial strain and the two local shears, while those of the angular 3-D vector represent the local torsional and flexural strains.

Given the definitions of the *sectional convected generalized inertia tensor* $\overline{\mathbf{M}}$ and of the *sectional convected generalized stiffness tensor* $\overline{\mathbf{K}}$, both symmetric and constant in time, we may write the constitutive equations for the beam as

$$\mathbf{p} := \mathbf{C}^{-T}\overline{\mathbf{M}}\,\overline{\mathbf{w}}, \qquad \mathbf{c} := \mathbf{C}^{-T}\overline{\mathbf{K}}\,\overline{\boldsymbol{\varepsilon}}, \tag{34}$$

where $\mathbf{p}$ is the *sectional base pole generalized kinetic moment* and $\mathbf{c}$ is the *sectional generalized stress resultant*. Consequently, the *kinetic energy* T and the *deformation energy* U may be written as

$$T := \frac{1}{2}\int_0^L \overline{\mathbf{w}} \cdot \overline{\mathbf{M}}\,\overline{\mathbf{w}}\,\mathrm{d}s, \qquad U := \frac{1}{2}\int_0^L \overline{\boldsymbol{\varepsilon}} \cdot \overline{\mathbf{K}}\,\overline{\boldsymbol{\varepsilon}}\,\mathrm{d}s. \tag{35}$$

In the case of a beam we distinguish two contributions to the resultant base pole generalized force $\mathbf{f}$: a base pole generalized *body force* with density $\mathbf{b}$ and a base pole generalized *contact force* with values $\mathbf{c}_0$ and $\mathbf{c}_L$ acting on the boundaries. The base pole dynamic balance equation is then expressed by

$$\frac{\mathrm{d}}{\mathrm{d}t}\int_0^L \mathbf{p}\,\mathrm{d}s = \int_0^L \mathbf{b}\,\mathrm{d}s + \mathbf{c}\big|_0^L \,. \tag{36}$$

A weak form of the balance equation may be obtained by projecting the local (i.e. differential) form of the dynamic balance at the base pole, $\dot{\mathbf{p}} - \mathbf{c}' = \mathbf{b}$, onto test functions $\boldsymbol{\pi}(s)$ and integrating along the beam. This procedure, after integration by parts, yields

$$\frac{\mathrm{d}}{\mathrm{d}t}\int_0^L \boldsymbol{\pi}\cdot\mathbf{p}\,\mathrm{d}s + \int_0^L \boldsymbol{\pi}'\cdot\mathbf{c}\,\mathrm{d}s = \int_0^L \boldsymbol{\pi}\cdot\mathbf{b}\,\mathrm{d}s + (\boldsymbol{\pi}\cdot\mathbf{c})|_0^L\,. \tag{37}$$

This general form can be used for developing finite-element or finite-volume semi-discretization processes.

2.2.3. Holonomic multibody system dynamics

We consider a general multibody system composed of both rigid and deformable bodies (elastic beams) linked via holonomic constraints. We limit ourselves to *ideal* constraints, i.e. constraints that produce reactions that perform null work for any admissible virtual displacement.

In this framework, the following equations, cast in the 6-D compact representation, represent the starting point for the development of the numerical methods presented in the following,

$$\frac{\mathrm{d}}{\mathrm{d}t}\mathbf{C} = \mathbf{C}\,\overline{\mathbf{w}}^{\times}, \tag{38}$$

$$\frac{\mathrm{d}}{\mathrm{d}t}\left(\mathbf{C}^{-T}\overline{\mathbf{M}}\,\overline{\mathbf{w}}\right) = \mathbf{f} + \mathbf{A}\,\boldsymbol{\lambda}, \tag{39}$$

$$\frac{\mathrm{d}}{\mathrm{d}t}\int_0^L \boldsymbol{\pi}\cdot\mathbf{C}^{-T}\overline{\mathbf{M}}\,\overline{\mathbf{w}}\,\mathrm{d}s + \int_0^L \boldsymbol{\pi}'\cdot\mathbf{C}^{-T}\overline{\mathbf{K}}\,\overline{\boldsymbol{\varepsilon}}\,\mathrm{d}s = \int_0^L \boldsymbol{\pi}\cdot\mathbf{b}\,\mathrm{d}s + (\boldsymbol{\pi}\cdot\mathbf{c})|_0^L + (\boldsymbol{\pi}\cdot\mathbf{A}\,\boldsymbol{\lambda})|_0^L. \tag{40}$$

$$\boldsymbol{\phi} = \mathbf{0}. \tag{41}$$

Equation (38) describes the time evolution of the configuration of the frames representing rigid bodies and beam sections. Equation (39) states the base pole dynamic balance equation for a rigid body subjected to ideal holonomic constraints. The latter are accounted for by the addition of generalized reaction force terms via Lagrangian multipliers $\boldsymbol{\lambda} \in \mathbb{R}^K$. Equation (40) states the base pole dynamic balance equation for a beam subjected to ideal holonomic constraints at its tips, in weak form. Again, the presence of holonomic constraints is accounted for via Lagrangian multipliers. Finally, Eq. (41) is the configuration-level algebraic equation that imposes an holonomic constraint between two material frames.

Note that we chose the moving frame version of the kinematic evolution equation (3) to exploit the advantages of using constant-in-time convected generalized inertia and stiffness tensors in the dynamic balance equations.

2.3. Cayley's parameterization

Cayley's parameterization of motion is based on *Cayley's transform*. This is a map acting on linear operators defined by the formula

$$\mathrm{cay}(\bullet) = (\mathbf{I} + \bullet)\,(\mathbf{I} - \bullet)^{-1}. \tag{42}$$

Remarkably, when $\bullet$ is in the Lie algebra $\mathrm{so}(\mathbb{E}^3)$ or $\mathrm{sr}(\mathbb{K}^6)$, the resulting $\mathrm{cay}(\bullet)$ is in the Lie group $\mathrm{SO}(\mathbb{E}^3)$ or $\mathrm{SR}(\mathbb{K}^6)$. Clearly, $\mathrm{cay}(\mathbf{O}) = \mathbf{I}$, where $\mathbf{O}$ and $\mathbf{I}$ are the null and the identity tensors in the relevant vector space. The inverse map is

$$\mathrm{cay}^{-1}(\star) = (\star - \mathbf{I})\,(\star + \mathbf{I})^{-1}, \tag{43}$$

so that the following fundamental properties hold

$$\text{cay}(\bullet)^{-1} = \text{cay}(-\bullet), \qquad \text{cay}^{-1}(\bullet) = -\text{cay}(-\bullet). \tag{44}$$

An *associated differential map*, symbolically defined as

$$\text{dcay}(\bullet) := \frac{\text{cay}(\bullet) - \mathbf{I}}{\bullet}. \tag{45}$$

may be introduced in the cases of rotation, $\bullet \in \text{so}(\mathbb{E}^3)$, as well as in the case of complete frame motion, $\bullet \in \text{sr}(\mathbb{K}^6)$. The explicit expression of this map will be given in the following. At this point we simply remark that Cayley's transform and its associated differential map satisfy the following general properties

$$\text{cay}(\bullet) = \text{dcay}(\bullet)\,\text{dcay}(-\bullet)^{-1}, \qquad \text{cay}(\bullet) = \mathbf{I} + \text{dcay}(\bullet)\,\bullet, \tag{46}$$

regardless of their application to the case either of rotation, or of complete frame motion.

2.3.1. Parameterization of rotation

Given any rotation tensor $\mathbf{R} \in \text{SO}(\mathbb{E}^3)$,

$$\mathbf{R} = \mathbf{I} + \sin\varphi\,(\mathbf{e}\times) + (1 - \cos\varphi)\,(\mathbf{e}\times)^2, \tag{47}$$

characterized by a rotation axis with unit vector $\mathbf{e} \in \mathbb{E}^3$ and a rotation angle $\varphi \in [0, 2\pi]$, we can find its *Cayley rotation vector* $\boldsymbol{\zeta} \in \mathbb{E}^3$ as the vector that satisfies

$$\mathbf{R} = \text{cay}(\boldsymbol{\zeta}\times), \tag{48}$$

with $\zeta := \|\boldsymbol{\zeta}\| = \tan\varphi/2$. Cayley's rotation vector $\boldsymbol{\zeta}$ represents then the parameter vector in Cayley's parameterization of rotations.[3] This can also be seen as the eigenvector corresponding to the unique real eigenvalue equal to $+1$ of the rotation tensor $\mathbf{R}$,

$$\mathbf{R}\,\boldsymbol{\zeta} = \boldsymbol{\zeta}. \tag{49}$$

The general expression in Eq. (42) reduces, in the case of rotation, to the formula

$$\mathbf{R} = \mathbf{I} + A(\zeta)\,(\mathbf{I} + \boldsymbol{\zeta}\times)\,\boldsymbol{\zeta}\times, \tag{50}$$

obtained exploiting the recursive properties of the cross product. The scalar coefficient $A(\zeta)$ is given by

$$A(\zeta) := \frac{2}{1 + \zeta^2}, \tag{51}$$

so that its value in terms of the rotation angle φ is $A = 2\cos^2(\varphi/2) = (1 + \cos\varphi)$. The differential tensor associated to $\mathbf{R}$, denoted by $\mathbf{Y} \in \text{Lin}(\mathbb{E}^3)$,

$$\mathbf{Y} := \text{dcay}(\boldsymbol{\zeta}\times), \tag{52}$$

is written as

$$\mathbf{Y} = A(\zeta)\,(\mathbf{I} + \boldsymbol{\zeta}\times). \tag{53}$$

[3] This technique is also variously named after Rodrigues or Gibbs, sometimes with the addition of a 'normalization' factor: in fact, some authors define the Gibbs-Rodrigues parameter vector as $2\,\boldsymbol{\zeta}$, to get $\zeta \longrightarrow \varphi$ as $\varphi \longrightarrow 0$.

This tensor relates the derivatives of $\mathbf{R}$ with those of $\boldsymbol{\zeta}$. In fact, it may be shown that

$$\dot{\mathbf{R}} = (\mathbf{Y}\,\dot{\boldsymbol{\zeta}}) \times \mathbf{R}. \tag{54}$$

The determinant of tensor $\mathbf{Y}$ is given by $\det(\mathbf{Y}) = 2\,A^2$ and its inverse reads

$$\mathbf{Y}^{-1} = \frac{1}{2}\Big(\mathbf{I} - (\boldsymbol{\zeta}\times) + \boldsymbol{\zeta}\otimes\boldsymbol{\zeta}\Big), \tag{55}$$

Note that no transcendental functions are involved in the expressions of Eqs. (50), (51), (53), (55), a possible computational advantage.

Using this parameterization, simple analytical expressions hold for the composition of rotations. In fact, given two successive rotations $\mathbf{R}_1 = \mathrm{cay}(\boldsymbol{\zeta}_1\times)$ and $\mathbf{R}_2 = \mathrm{cay}(\boldsymbol{\zeta}_2\times)$, the Cayley rotation vector $\boldsymbol{\zeta} := \mathrm{axial}_\times(\mathrm{cay}^{-1}(\mathbf{R}))$ corresponding to the resulting rotation tensor $\mathbf{R} := \mathbf{R}_2\,\mathbf{R}_1$ is given by the following equation,

$$\boldsymbol{\zeta} = \frac{1}{1 - \boldsymbol{\zeta}_1\cdot\boldsymbol{\zeta}_2}(\boldsymbol{\zeta}_2 + \boldsymbol{\zeta}_1 + \boldsymbol{\zeta}_2\times\boldsymbol{\zeta}_1), \tag{56}$$

which is known as *Rodrigues' formula*. For later convenience, let us rewrite the preceding equation in terms of the sum and difference of the component vectors $\boldsymbol{\zeta}_1$, $\boldsymbol{\zeta}_2$ as

$$\boldsymbol{\zeta} = \lambda\,\mathbf{L}\,(\boldsymbol{\zeta}_2 + \boldsymbol{\zeta}_1), \tag{57}$$

where we defined the scalar and tensor coefficients λ and $\mathbf{L}$ as

$$\lambda := \frac{1}{1 - \boldsymbol{\zeta}_1\cdot\boldsymbol{\zeta}_2}, \qquad \mathbf{L} := \mathbf{I} + \frac{1}{2}(\boldsymbol{\zeta}_2 - \boldsymbol{\zeta}_1)\times, \tag{58}$$

respectively.

2.3.2. Parameterization of frame motion

Given any displacement tensor $\mathbf{D} \in \mathrm{SR}(\mathbb{K}^6)$,

$$\mathbf{D} = \begin{bmatrix} \mathbf{R} & \mathbf{t}\times\mathbf{R} \\ \mathbf{O} & \mathbf{R} \end{bmatrix}, \tag{59}$$

characterized by a rotation tensor $\mathbf{R} \in \mathrm{SO}(\mathbb{E}^3)$ and a translation vector $\mathbf{t} \in \mathbb{E}^3$, we can find its *Cayley displacement vector* $\boldsymbol{\eta} \in \mathbb{K}^6$ as the 6-D vector that satisfies

$$\mathbf{D} = \mathrm{cay}(\boldsymbol{\eta}\times). \tag{60}$$

It may be easily shown that $\boldsymbol{\eta} = (\boldsymbol{\gamma}; \boldsymbol{\zeta})$, where the angular 3-D component $\boldsymbol{\zeta}$ coincides with the Cayley rotation vector corresponding to $\mathbf{R}$, while the linear 3-D component is $\boldsymbol{\gamma} = \mathbf{Y}^{-1}\mathbf{t}$ where $\mathbf{Y} := \mathrm{dcay}(\boldsymbol{\zeta}\times)$ is the differential tensor associated to $\mathbf{R}$.

Cayley's displacement vector $\boldsymbol{\eta}$ represents then the parameter vector in Cayley's parameterization of motion. It can also be seen as the eigenvector corresponding to the unique real eigenvalue equal to $+1$ of the displacement tensor $\mathbf{D}$,

$$\mathbf{D}\,\boldsymbol{\eta} = \boldsymbol{\eta}. \tag{61}$$

The general expression in Eq. (42) reduces, in the case of frame motion, to the formula

$$\mathbf{D} = \mathbf{I} + \hat{\mathbf{A}}(\vartheta, \boldsymbol{\zeta})\,(\mathbf{I} + \boldsymbol{\eta}\times)\,\boldsymbol{\eta}\times, \tag{62}$$

obtained exploiting the recursive properties of the North-East generalized cross product. The tensorial coefficient $\hat{\mathbf{A}}(\vartheta,\zeta)$ is given by

$$\hat{\mathbf{A}}(\vartheta,\zeta) := A(\zeta)\begin{bmatrix} \mathbf{I} & -\vartheta\,\zeta^2 A(\zeta)\,\mathbf{I} \\ \mathbf{O} & \mathbf{I} \end{bmatrix}, \tag{63}$$

where we have defined the scalar ϑ, termed the *pitch* of $\boldsymbol{\eta}$, as

$$\vartheta := \frac{\boldsymbol{\gamma}\cdot\boldsymbol{\zeta}}{\zeta^2}. \tag{64}$$

The differential tensor associated to $\mathbf{D}$, denoted by $\mathbf{Z} \in \mathrm{Lin}(\mathbb{K}^6)$,

$$\mathbf{Z} := \mathrm{dcay}(\boldsymbol{\eta}\times), \tag{65}$$

is written as

$$\mathbf{Z} = \hat{\mathbf{A}}(\vartheta,\zeta)\,(\mathbf{I} + \boldsymbol{\eta}\times). \tag{66}$$

This tensor relates the derivatives of $\mathbf{D}$ with those of $\boldsymbol{\eta}$ in close analogy to the rotation case. In fact, it may be shown that

$$\dot{\mathbf{D}} = (\mathbf{Z}\,\dot{\boldsymbol{\eta}})\times\mathbf{D}. \tag{67}$$

The inverse of tensor $\mathbf{Z}$ is given by

$$\mathbf{Z}^{-1} = \frac{1}{2}\Big(\mathbf{I} - (\boldsymbol{\eta}\times) + \boldsymbol{\eta}\otimes\boldsymbol{\eta}\Big), \tag{68}$$

where the symbol $\otimes$, introduced to stress the formal analogy with Eq. (55), indicates a 6-D tensor product defined as

$$\boldsymbol{\eta}_1\otimes\boldsymbol{\eta}_2 := \begin{bmatrix} \boldsymbol{\zeta}_1\otimes\boldsymbol{\zeta}_2 & (\boldsymbol{\gamma}_1\otimes\boldsymbol{\zeta}_2 + \boldsymbol{\zeta}_1\otimes\boldsymbol{\gamma}_2) \\ \mathbf{O} & \boldsymbol{\zeta}_1\otimes\boldsymbol{\zeta}_2 \end{bmatrix}. \tag{69}$$

Again we end up with remarkably simple expressions in Eqs. (62), (63), (66), (68) where no transcendental functions are involved, and again we recover the simple, analytical expression in the case of the composition of rigid displacements.

In fact, given two successive displacements $\mathbf{D}_1 = \mathrm{cay}(\boldsymbol{\eta}_1\times)$ and $\mathbf{D}_2 = \mathrm{cay}(\boldsymbol{\eta}_2\times)$, the Cayley displacement vector $\boldsymbol{\eta} := \mathrm{axial}_\times(\mathrm{cay}^{-1}(\mathbf{D}))$ corresponding to the resulting displacement tensor $\mathbf{D} := \mathbf{D}_2\,\mathbf{D}_1$ is given by the following equation,

$$\boldsymbol{\eta} = \frac{1}{1-\boldsymbol{\zeta}_1\cdot\boldsymbol{\zeta}_2}\begin{bmatrix} \mathbf{I} & \dfrac{\boldsymbol{\gamma}_1\cdot\boldsymbol{\zeta}_2 + \boldsymbol{\gamma}_2\cdot\boldsymbol{\zeta}_1}{1-\boldsymbol{\zeta}_1\cdot\boldsymbol{\zeta}_2}\,\mathbf{I} \\ \mathbf{O} & \mathbf{I} \end{bmatrix}(\boldsymbol{\eta}_2 + \boldsymbol{\eta}_1 + \boldsymbol{\eta}_2\times\boldsymbol{\eta}_1), \tag{70}$$

which is the 6-D generalization of Rodrigues' formula. This equation may be rewritten in terms of the sum and difference of the component vectors $\boldsymbol{\eta}_1$, $\boldsymbol{\eta}_2$ as

$$\boldsymbol{\eta} = \boldsymbol{\Lambda}\,\hat{\mathbf{L}}\,(\boldsymbol{\eta}_2 + \boldsymbol{\eta}_1), \tag{71}$$

where the tensorial coefficients $\boldsymbol{\Lambda}$ and $\hat{\mathbf{L}}$ are defined as

$$\boldsymbol{\Lambda} := \lambda\begin{bmatrix} \mathbf{I} & \mu\,\mathbf{I} \\ \mathbf{O} & \mathbf{I} \end{bmatrix}, \qquad \hat{\mathbf{L}} := \mathbf{I} + \frac{1}{2}(\boldsymbol{\eta}_2 - \boldsymbol{\eta}_1)\times, \tag{72}$$

while $\mu := (\boldsymbol{\gamma}_1\cdot\boldsymbol{\zeta}_2 + \boldsymbol{\gamma}_2\cdot\boldsymbol{\zeta}_1)/(1-\boldsymbol{\zeta}_1\cdot\boldsymbol{\zeta}_2)$.

As it is apparent from the preceding developments, Cayley's parameterization of motion retains all of the advantages that make its well known 3-D version for rotation a convenient and widely adopted computational tool.

2.3.3. *Frame kinematic evolution equations*

In view of the development of the numerical integration schemes, the use of Cayley's parameterization of motion requires the replacement of the evolution equation (38) for the frame configuration tensors with the updates

$$\mathbf{C} = \mathrm{cay}(\boldsymbol{\eta}^{\times})\,\mathbf{C}_0, \qquad \mathbf{C} = \mathbf{C}_0\,\mathrm{cay}(\overline{\boldsymbol{\eta}}^{\times}), \tag{73}$$

together with the evolution equation for the corresponding Cayley displacement vector $\boldsymbol{\eta}$ or $\overline{\boldsymbol{\eta}}$ from $\mathbf{C}_0$ to $\mathbf{C}$, as derived from Eq. (67),

$$\dot{\boldsymbol{\eta}} = \mathrm{dcay}(\boldsymbol{\eta}^{\times})^{-1}\mathbf{w}, \qquad \dot{\overline{\boldsymbol{\eta}}} = \mathrm{dcay}(-\overline{\boldsymbol{\eta}}^{\times})^{-1}\overline{\mathbf{w}}. \tag{74}$$

The constant-in-time configuration tensor $\mathbf{C}_0 \in \mathrm{SR}(\mathbb{K}^6)$ is taken as a reference value. In particular, we shall select $\mathbf{C}_0 = \mathbf{C}^n$ at each time step $[t_n, t_{n+1}]$, considering thus *incremental* displacements. Also, we shall select the second version of each of the above equations (the 'convected' version instead of the 'base pole' version) for the numerical schemes proposed next.

3. Non-linearly unconditionally stable algorithms

Numerical solution schemes will now be developed based on discretizations of Eqs. (73), (74), (39), (40) and (41). First, the *momentum and energy preserving scheme*, labeled the MP-EP scheme, will be derived. The MP-EP scheme features non-linear unconditional stability due to an algorithmic law of energy conservation, in addition to the conservation of the total fixed pole momentum and the property of geometric invariance. Next, the *momentum preserving, energy decaying scheme*, hereafter labeled the MP-ED scheme, will be obtained. The MP-ED scheme retains all the properties of the MP-EP scheme, while replacing energy preservation with strict decay within each time step.

3.1. Momentum and energy preserving algorithm

3.1.1. *Basic equations*

A second order accurate numerical integration scheme capable of preserving both the total linear and angular momenta with respect to a fixed pole, together with the total mechanical energy of a holonomically constrained flexible multibody system is based on the following discrete equations:

$$\mathbf{C}^{n+1} = \mathbf{C}^n\,\mathrm{cay}(\overline{\boldsymbol{\eta}}^{n+1\times}), \tag{75}$$

$$\overline{\boldsymbol{\eta}}^{n+1} = \frac{h_n}{4}\left(\overline{\mathbf{w}}^n + \overline{\mathbf{w}}^{n+1}\right), \tag{76}$$

$$\mathbf{C}^{n+1-T}\overline{\mathbf{M}}\,\overline{\mathbf{w}}^{n+1} = \mathbf{C}^{n-T}\overline{\mathbf{M}}\,\overline{\mathbf{w}}^{n} + \frac{h_n}{2}(\mathbf{f}^n + \mathbf{f}^{n+1}) + h_n\,\mathbf{A}^m\boldsymbol{\lambda}^m, \tag{77}$$

$$\begin{aligned}\int_0^L \boldsymbol{\pi}\cdot\mathbf{C}^{n+1-T}\overline{\mathbf{M}}\,\overline{\mathbf{w}}^{n+1}\,\mathrm{d}s &= \int_0^L \boldsymbol{\pi}\cdot\mathbf{C}^{n-T}\overline{\mathbf{M}}\,\overline{\mathbf{w}}^{n}\,\mathrm{d}s \\ &- \frac{h_n}{2}\int_0^L \boldsymbol{\pi}'\cdot(\mathbf{C}^{n-T}\overline{\mathbf{K}}\,\overline{\boldsymbol{\varepsilon}}^n + \mathbf{C}^{n+1-T}\overline{\mathbf{K}}\,\overline{\boldsymbol{\varepsilon}}^{n+1})\,\mathrm{d}s + \frac{h_n}{2}\int_0^L \boldsymbol{\pi}\cdot(\mathbf{b}^n + \mathbf{b}^{n+1})\,\mathrm{d}s \\ &+ \frac{h_n}{2}\left(\boldsymbol{\pi}\cdot(\mathbf{c}^n + \mathbf{c}^{n+1})\right)\Big|_0^L + h_n\left(\boldsymbol{\pi}\cdot\mathbf{A}^m\boldsymbol{\lambda}^m\right)\Big|_0^L,\end{aligned} \tag{78}$$

$$\boldsymbol{\phi}^{n+1} = \mathbf{0}, \tag{79}$$

within the time step $[t_n, t_{n+1}]$ with $h_n := t_{n+1} - t_n$. The first two Eqs. (75) and (76) are written for the N^r rigid bodies in addition to the N^n nodes of the discretized flexible bodies. Equation (77) is

written for the N^r rigid bodies, while Eq. (78) for the N^e elements of the discretized flexible bodies. Finally, Eq. (79) is written for the N^c constrained frame pairs.

The discrete multiplicative update formula (75) prevents the integration of the configuration tensors from drifting from the manifold $\mathrm{SR}(\mathbb{K}^6)$. Together with the evolution equation for the Cayley displacement vector (76), the update formula defines $\overline{\boldsymbol{\eta}}^{n+1}$ as an incremental quantity, null at the beginning of each time step. The incremental approach allows to avoid the difficulty related to the singularity of the parameterization of rotation embedded in the global parameterization of motion adopted here.

The constraint reaction forces in the dynamic balance equations (77) and (78) are discretized resorting to suitable 'averages' expressed by the combination of a constraint tensor $\mathbf{A}^m$ and a corresponding Lagrangian multiplier $\boldsymbol{\lambda}^m$. The averaged constraint tensor $\mathbf{A}^m$ is designed to meet a particular stability requirement, as it will be shown in the following. Note that, when considering a constrained frame pair composed of frames A and B, the multipliers relative to bodies $\mathcal{B}_A$ and $\mathcal{B}_B$ are assumed equal in magnitude and direction, and opposite in sign, i.e. $\boldsymbol{\lambda}^m = -\boldsymbol{\lambda}^m_A \equiv +\boldsymbol{\lambda}^m_B$. The generalized reaction forces acting on these bodies are then given by $-\mathbf{A}^m_A\,\boldsymbol{\lambda}^m$ and $+\mathbf{A}^m_B\,\boldsymbol{\lambda}^m$, respectively. Clearly, the resulting N^c averaged Lagrangian multiplier vectors represent additional unknowns with respect to the unconstrained case.

This MP-EP method may be seen as a modified *Trapezoidal Rule* applied to Eqs. $(74)_2$, (39) and (40), where the discretized form of Eq. $(74)_2$ is substituted by an approximation obtained truncating the value of $\mathrm{dcay}(\overline{\boldsymbol{\eta}}^{n+1}\times)^{-1}$ to the first term of its series expansion with respect to $(\overline{\boldsymbol{\eta}}^{n+1}\times)$. In conclusion, since we enforce the constraint equation (79) at the end of the time step, we get a DAE integrator that, given that the initial conditions comply with the imposed constraint, exactly maintains the solution on the configuration manifold of the system, i.e. no constraint *drift* can take place.

3.1.2. Preservation of energy

The MP-EP scheme described above displays non-linear unconditional stability based on the energy method. In fact, a *discrete total mechanical energy conservation law* is algorithmically implied by the above equations. This may be easily proved in two steps. First, we obtain an expression for the difference of the total mechanical energy of the system in terms of the discrete work of the applied and reaction generalized forces. Then we prove that, assuming a suitable expression of the averaged constraint tensors, the work performed by the constraint reactions vanishes for time-independent ideal constraints. These steps are detailed in [7, 9] and shall be briefly recalled here.

Variation of mechanical energy within the time step

We conjugate Eq. (77) with the 'average generalized velocity' $2\,\boldsymbol{\eta}^{n+1}/h_n$, obtaining

$$T^{n+1} - T^n = \boldsymbol{\eta}^{n+1} \cdot (\mathbf{f}^n + \mathbf{f}^{n+1}) + \boldsymbol{\eta}^{n+1} \cdot 2\,\mathbf{A}^m \boldsymbol{\lambda}^m, \tag{80}$$

which can be seen as a discretized form of the kinetic energy conservation theorem holding for each of the N^r rigid bodies. Similarly, denoting with $E := T + U$ the total mechanical energy of the beams, by substituting $2\,\boldsymbol{\eta}^{n+1}/h_n$ to the generic test function $\boldsymbol{\pi}$ in Eq. (78), we get

$$E^{n+1} - E^n = \int_0^L \boldsymbol{\eta}^{n+1} \cdot (\mathbf{b}^n + \mathbf{b}^{n+1})\,\mathrm{d}s + \left(\boldsymbol{\eta}^{n+1} \cdot (\mathbf{c}^n + \mathbf{c}^{n+1})\right)\Big|_0^L + \left(\boldsymbol{\eta}^{n+1} \cdot 2\,\mathbf{A}^m \boldsymbol{\lambda}^m\right)\Big|_0^L, \tag{81}$$

which can analogously be seen as a discretized form of the total mechanical energy conservation theorem holding for each of the N^e beam elements. Note that this property holds regardless of the particular semi-discretization employed. This result is achieved by assuming a convenient discretization of the resultant internal forces within the time step $(\mathbf{c}^n + \mathbf{c}^{n+1})$ in such a way that it properly matches the expression of the generalized strains as recovered from the spatial distribution of the generalized displacement vector (see [7, 9, 10]).

In the absence of applied loads, i.e. $\mathbf{f} = \mathbf{b} = \mathbf{c} = \mathbf{0}$, the variation of the total mechanical energy of the whole multibody system in a time step is equal to the sum of the work performed by the constraint reaction forces, i.e. the second and third terms at the right hand side of Eqs. (80) and (81), respectively.

Work of the constraint reaction forces within the time step

To obtain full non-linear unconditional stability according to the energy method we need a particular stability requirement on the discretization of the constraint reaction forces. Time-independent ideal constraints give rise to reaction forces that do not perform any work. Therefore, we require our scheme to inherit this fundamental feature in a discrete sense, so that, when the constraints are ideal and time-independent, the algorithmic reaction forces perform null work within the time step.

Let us refer to a pair of mutually constrained bodies $\mathcal{B}_A$ and $\mathcal{B}_B$, linked by a holonomic constraint $\boldsymbol{\phi} = \mathbf{0}$ (for the sake of brevity, we shall consider both of them as rigid bodies). We design the averaged constraint tensors $\mathbf{A}_A^m$ and $\mathbf{A}_B^m$ in such a way that

$$\mathbf{A}_B^{mT}\boldsymbol{\eta}_B^{n+1} - \mathbf{A}_A^{mT}\boldsymbol{\eta}_A^{n+1} = \boldsymbol{\phi}^{n+1} - \boldsymbol{\phi}^n. \tag{82}$$

In fact, this yields

$$\boldsymbol{\eta}_B^{n+1} \cdot \mathbf{A}_B^m \boldsymbol{\lambda}^m - \boldsymbol{\eta}_A^{n+1} \cdot \mathbf{A}_A^m \boldsymbol{\lambda}^m = 0, \tag{83}$$

being the left-hand side equal to $(\boldsymbol{\phi}^{n+1} - \boldsymbol{\phi}^n) \cdot \boldsymbol{\lambda}^m$, and $\boldsymbol{\phi}^n = \mathbf{0}$ at the end of the preceding time step. Thus, the averaged constraint reaction forces on bodies $\mathcal{B}_A$ and $\mathcal{B}_A$ perform equal and opposite algorithmic work over the generalized displacements $\boldsymbol{\eta}_A^{n+1}$ and $\boldsymbol{\eta}_B^{n+1}$, yielding the vanishing of the total reaction work for the body pair. From Eq. (80) we get the conservation statement for the kinetic energy of the rigid body pair given as

$$(T_A^{n+1} + T_B^{n+1}) - (T_A^n + T_B^n) = \boldsymbol{\eta}_B^{n+1} \cdot \left(\mathbf{f}_B^{An} + \mathbf{f}_B^{An+1}\right) + \boldsymbol{\eta}_A^{n+1} \cdot \left(\mathbf{f}_A^{An} + \mathbf{f}_A^{An+1}\right), \tag{84}$$

and, consequently, the total mechanical energy of the system is exactly preserved in the absence of applied loads.

Design of conservative averaged constraint tensors

To comply with the design requirement expressed by Eq. (82), the increment $\boldsymbol{\phi}^{n+1} - \boldsymbol{\phi}^n$ in the configuration-level constraint must be expressed in terms of the Cayley displacement vectors $\boldsymbol{\eta}_A^{n+1}$ and $\boldsymbol{\eta}_B^{n+1}$ corresponding to the configuration updates

$$\mathbf{C}_A^{n+1} = \mathrm{cay}(\boldsymbol{\eta}_A^{n+1\times})\,\mathbf{C}_A^n, \qquad \mathbf{C}_B^{n+1} = \mathrm{cay}(\boldsymbol{\eta}_B^{n+1\times})\,\mathbf{C}_B^n, \tag{85}$$

respectively. We define a *relative incremental displacement vector* $\boldsymbol{\eta}_\varepsilon^{n+1} = (\boldsymbol{\gamma}_\varepsilon^{n+1}; \boldsymbol{\zeta}_\varepsilon^{n+1})$ for each constrained frame pair as the Cayley displacement vector corresponding to $\mathrm{cay}(\boldsymbol{\eta}_\varepsilon^{n+1\times}) = \mathrm{cay}(\boldsymbol{\eta}_A^{n+1})^{-1}\mathrm{cay}(\boldsymbol{\eta}_B^{n+1})$. This vector can be obtained directly by the 6-D extension (71) of Rodrigues formula as

$$\boldsymbol{\eta}_\varepsilon^{n+1} = \boldsymbol{\Lambda}^{n+1}\,\hat{\mathbf{L}}^{n+1}(\boldsymbol{\eta}_B^{n+1} - \boldsymbol{\eta}_A^{n+1}), \tag{86}$$

with

$$\boldsymbol{\Lambda}^{n+1} := \lambda^{n+1}\begin{bmatrix} \mathbf{I} & \mu^{n+1}\mathbf{I} \\ \mathbf{O} & \mathbf{I} \end{bmatrix}, \qquad \hat{\mathbf{L}}^{n+1} := \left(\mathbf{I} - \frac{1}{2}(\boldsymbol{\eta}_A^{n+1} + \boldsymbol{\eta}_B^{n+1})^\times\right), \tag{87}$$

where $\lambda^{n+1} := 1/(1 + \boldsymbol{\zeta}_A^{n+1} \cdot \boldsymbol{\zeta}_B^{n+1})$ and $\mu^{n+1} := -(\boldsymbol{\gamma}_A^{n+1} \cdot \boldsymbol{\zeta}_B^{n+1} + \boldsymbol{\gamma}_B^{n+1} \cdot \boldsymbol{\zeta}_A^{n+1})/(1 + \boldsymbol{\zeta}_A^{n+1} \cdot \boldsymbol{\zeta}_B^{n+1})$. We resort to $\boldsymbol{\eta}_\varepsilon^{n+1}$ since all the basic holonomic constraints may be expressed in incremental form as

$$\boldsymbol{\phi}^{n+1} - \boldsymbol{\phi}^n = \mathbf{G}^{n+1^T}\boldsymbol{\eta}_\varepsilon^{n+1}, \tag{88}$$

through a suitable *incremental constraint tensor* $\mathbf{G}^{n+1}$. This means that a single 'averaged' constraint tensor $\mathbf{A}^m = \mathbf{A}^m_A \equiv \mathbf{A}^m_B$ may be assumed simply as

$$\mathbf{A}^m := \mathbf{\Lambda}^{n+1^T} \hat{\mathbf{L}}^{n+1^T} \mathbf{G}^{n+1}. \tag{89}$$

This expression for $\mathbf{A}^m$ satisfies by construction the design requirement (82), and represents a reasonable approximation of $\mathbf{A}$ within the time step from t_n to t_{n+1}, even if it does not necessarily coincide with any value assumed by $\mathbf{A}$ for any $t \in [t_n, t_{n+1}]$.

Examples of the incremental constraint tensor $\mathbf{G}^{n+1}$ are given below for the previously considered prismatic joint $\mathcal{J}_\mathcal{P}$ and revolute joint $\mathcal{J}_\mathcal{R}$,

$$\mathbf{G}^{n+1}_\mathcal{P} = \begin{bmatrix} \mathbf{Y}^T_\varepsilon \mathbf{e}^n_{A1} & \mathbf{Y}^T_\varepsilon \mathbf{e}^n_{A2} & \mathbf{O} \\ \mathbf{u}^n_B \times \mathbf{Y}^T_\varepsilon \mathbf{e}^n_{A1} & \mathbf{u}^n_B \times \mathbf{Y}^T_\varepsilon \mathbf{e}^n_{A2} & \mathbf{e}^n_{B3} \times \mathbf{Y}^T_\varepsilon \end{bmatrix}, \tag{90}$$

$$\mathbf{G}^{n+1}_\mathcal{R} = \begin{bmatrix} \mathbf{Y}^T_\varepsilon & \mathbf{0} & \mathbf{0} \\ \mathbf{u}^n_B \times \mathbf{Y}^T_\varepsilon & \mathbf{e}^n_{B3} \times \mathbf{Y}^T_\varepsilon \mathbf{e}^n_{A1} & \mathbf{e}^n_{B3} \times \mathbf{Y}^T_\varepsilon \mathbf{e}^n_{A2} \end{bmatrix}. \tag{91}$$

where $\mathbf{Y}_\varepsilon := \mathrm{dcay}(\boldsymbol{\zeta}^{n+1}_\varepsilon \times)$ is the differential tensor associated to the relative incremental rotation tensor $\mathrm{cay}(\boldsymbol{\zeta}^{n+1}_\varepsilon \times) = \mathrm{cay}(\boldsymbol{\zeta}^{n+1}_A)^{-1} \mathrm{cay}(\boldsymbol{\zeta}^{n+1}_B)$.

Formulae for the conservative averages of other holonomic constraints can be derived in a similar form.

3.1.3. Preservation of linear and angular momenta

For an unconstrained body, reduction to the base pole in the derivation of the dynamic balance equations (77) and (78) ensures the exact preservation at the discrete level of the linear and base pole angular momenta whenever the applied loading vanishes. Consider now the case of constrained bodies (a constrained rigid body is considered for the sake of brevity): from Eq. (77), whenever $\mathbf{f} = \mathbf{0}$, we get

$$\mathbf{p}^{n+1} - \mathbf{p}^n = h_n \, \mathbf{A}^m \boldsymbol{\lambda}^m, \tag{92}$$

with $\{\mathbf{p}^k = \mathbf{C}^{k^{-T}} \overline{\mathbf{M}} \, \overline{\mathbf{w}}^k\}_{k=n,n+1}$. This means that the possible lack of preservation of momenta lies in the difference between the reaction forces exerted among constrained body pairs. Generally speaking, a time discretization of such forces using average quantities does not ensure their balance within each constrained frame pair.

However, the strategy sketched above results in an algorithm that retains Newton's Third Law for each constrained body pair. In fact, Eqs. (82), (86), and (89) imply that the discretized constraint reaction forces acting on bodies $\mathcal{B}_A$ and $\mathcal{B}_B$ are equal in magnitude and direction, and opposite in sign, being $-\mathbf{A}^m \boldsymbol{\lambda}^m$ and $+\mathbf{A}^m \boldsymbol{\lambda}^m$, respectively. This implies that, considering a pair of mutually constrained rigid bodies, we get

$$(\mathbf{p}^{n+1}_A + \mathbf{p}^{n+1}_B) - (\mathbf{p}^n_A + \mathbf{p}^n_B) = \frac{h_n}{2}(\mathbf{f}^n_A + \mathbf{f}^{n+1}_A) + \frac{h_n}{2}(\mathbf{f}^n_B + \mathbf{f}^{n+1}_B). \tag{93}$$

Therefore, considering the base pole dynamic balance equations for each rigid body and beam element in the system, we get that in the case of load-free motion the total linear momentum and the total angular momentum with respect to the base pole (and hence with respect to any fixed pole) of the multibody system is exactly preserved.

3.2. Momentum preserving, energy decaying algorithm

3.2.1. Basic equations

The proposed numerical integration scheme, applied to the time step $[t_n, t_{n+1}]$, reads

$$\mathbf{C}^j = \mathbf{C}^n \operatorname{cay}(\overline{\boldsymbol{\eta}}^j \times), \tag{94}$$

$$\overline{\boldsymbol{\eta}}^j = \frac{h_n}{12}\left(\overline{\mathbf{w}}^j - \overline{\mathbf{w}}^{n+1}\right), \tag{95}$$

$$\mathbf{C}^{j-T}\overline{\mathbf{M}}\,\overline{\mathbf{w}}^j = \mathbf{C}^{n-T}\overline{\mathbf{M}}\,\overline{\mathbf{w}}^n + \frac{h_n}{6}(\mathbf{f}^j - \mathbf{f}^{n+1}) + h_n\,\mathbf{A}^h\boldsymbol{\lambda}^h, \tag{96}$$

$$\begin{aligned}\int_0^L \boldsymbol{\pi}\cdot\mathbf{C}^{j-T}\overline{\mathbf{M}}\,\overline{\mathbf{w}}^j\,\mathrm{d}s &= \int_0^L \boldsymbol{\pi}\cdot\mathbf{C}^{n-T}\overline{\mathbf{M}}\,\overline{\mathbf{w}}^n\,\mathrm{d}s \\ &- \frac{h_n}{6}\int_0^L \boldsymbol{\pi}'\cdot(\mathbf{C}^{j-T}\overline{\mathbf{K}}\,\overline{\boldsymbol{\varepsilon}}^j - \mathbf{C}^{n+1-T}\overline{\mathbf{K}}\,\overline{\boldsymbol{\varepsilon}}^{n+1})\,\mathrm{d}s + \frac{h_n}{6}\int_0^L \boldsymbol{\pi}\cdot(\mathbf{b}^j - \mathbf{b}^{n+1})\,\mathrm{d}s \\ &+ \frac{h_n}{6}\left(\boldsymbol{\pi}\cdot(\mathbf{c}^j - \mathbf{c}^{n+1})\right)\Big|_0^L + h_n\left(\boldsymbol{\pi}\cdot\mathbf{A}^h\boldsymbol{\lambda}^h\right)\Big|_0^L,\end{aligned} \tag{97}$$

$$\boldsymbol{\phi}^j = \mathbf{0}, \tag{98}$$

at the internal stage $t_j = t_n^+$, and

$$\mathbf{C}^{n+1} = \mathbf{C}^n \operatorname{cay}(\overline{\boldsymbol{\eta}}^{n+1} \times), \tag{99}$$

$$\overline{\boldsymbol{\eta}}^{n+1} = \frac{h_n}{4}\left(\overline{\mathbf{w}}^j + \overline{\mathbf{w}}^{n+1}\right), \tag{100}$$

$$\mathbf{C}^{n+1-T}\overline{\mathbf{M}}\,\overline{\mathbf{w}}^{n+1} = \mathbf{C}^{n-T}\overline{\mathbf{M}}\,\overline{\mathbf{w}}^n + \frac{h_n}{2}(\mathbf{f}^j + \mathbf{f}^{n+1}) + h_n\,\mathbf{A}^g\boldsymbol{\lambda}^g, \tag{101}$$

$$\begin{aligned}\int_0^L \boldsymbol{\pi}\cdot\mathbf{C}^{n+1-T}\overline{\mathbf{M}}\,\overline{\mathbf{w}}^{n+1}\,\mathrm{d}s &= \int_0^L \boldsymbol{\pi}\cdot\mathbf{C}^{n-T}\overline{\mathbf{M}}\,\overline{\mathbf{w}}^n\,\mathrm{d}s \\ &- \frac{h_n}{2}\int_0^L \boldsymbol{\pi}'\cdot(\mathbf{C}^{j-T}\overline{\mathbf{K}}\,\overline{\boldsymbol{\varepsilon}}^j + \mathbf{C}^{n+1-T}\overline{\mathbf{K}}\,\overline{\boldsymbol{\varepsilon}}^{n+1})\,\mathrm{d}s + \frac{h_n}{2}\int_0^L \boldsymbol{\pi}\cdot(\mathbf{b}^j + \mathbf{b}^{n+1})\,\mathrm{d}s \\ &+ \frac{h_n}{2}\left(\boldsymbol{\pi}\cdot(\mathbf{c}^j + \mathbf{c}^{n+1})\right)\Big|_0^L + h_n\left(\boldsymbol{\pi}\cdot\mathbf{A}^g\boldsymbol{\lambda}^g\right)\Big|_0^L,\end{aligned} \tag{102}$$

$$\boldsymbol{\phi}^{n+1} = \mathbf{0}, \tag{103}$$

at the step completion t_{n+1}.

This MP-ED method may be seen as a modification of the previously discussed MP-EP scheme, with the addition of an internal stage labeled with the superscript j, a remainder that a 'jump' discontinuity occurs between t_n and t_j. The scheme retains all the characteristics already discussed for the MP-EP scheme with respect to geometric integration, incremental updating, and constraint force averaging. It may also be considered as a modified Runge-Kutta method corresponding to a second-order (third-order in the linear case) *Time-Discontinuous Galerkin* scheme with vanishing spectral radius at infinity [9]. This scheme represents a DAE integrator with selective high-frequency algorithmic damping.

3.2.2. Energy decay

The MP-ED scheme described above enjoys non-linear unconditional stability based on the energy method. In fact, a *discrete total mechanical energy dissipation law* is algorithmically implied by the above equations. This may be easily proved resorting to similar arguments as for MP-EP case. The reader is addressed to [7, 9] for further details.

By conjugating Eq. (101) with $2\boldsymbol{\eta}^{n+1}/h_n$ and Eq. (96) with $6\boldsymbol{\eta}^{j}/h_n$ we obtain

$$T^{n+1} - T^n + \Delta_j T = \boldsymbol{\eta}^{n+1} \cdot (\mathbf{f}^j + \mathbf{f}^{n+1}) + \boldsymbol{\eta}^j \cdot (\mathbf{f}^j - \mathbf{f}^{n+1}) + \boldsymbol{\eta}^{n+1} \cdot 2\,\mathbf{A}^g \boldsymbol{\lambda}^g + \boldsymbol{\eta}^j \cdot 2\,\mathbf{A}^h \boldsymbol{\lambda}^h, \quad (104)$$

for each of the N^r rigid bodies. The strictly non-negative kinetic energy decay $\Delta_j T$ is easily expressed as

$$\Delta_j T := \frac{1}{2} (\overline{\mathbf{w}}^j - \overline{\mathbf{w}}^n) \cdot \overline{\mathbf{M}} (\overline{\mathbf{w}}^j - \overline{\mathbf{w}}^n). \quad (105)$$

With similar considerations we end up with

$$\begin{aligned} E^{n+1} - E^n + \Delta_j E = & \int_0^L \boldsymbol{\eta}^{n+1} \cdot (\mathbf{b}^j + \mathbf{b}^{n+1})\, \mathrm{d}s + \int_0^L \boldsymbol{\eta}^j \cdot (\mathbf{b}^j - \mathbf{b}^{n+1})\, \mathrm{d}s \\ & + \left(\boldsymbol{\eta}^{n+1} \cdot (\mathbf{c}^j + \mathbf{c}^{n+1})\right)\Big|_0^L + \left(\boldsymbol{\eta}^j \cdot (\mathbf{c}^j - \mathbf{c}^{n+1})\right)\Big|_0^L \\ & + \left(\boldsymbol{\eta}^{n+1} \cdot 2\,\mathbf{A}^g \boldsymbol{\lambda}^g\right)\Big|_0^L + \left(\boldsymbol{\eta}^j \cdot 2\,\mathbf{A}^h \boldsymbol{\lambda}^h\right)\Big|_0^L, \end{aligned} \quad (106)$$

for each of the N^e beam elements. The strictly non-negative total mechanical energy decay $\Delta_j E$ reads

$$\Delta_j E := \frac{1}{2} \int_0^L (\overline{\mathbf{w}}^j - \overline{\mathbf{w}}^n) \cdot \overline{\mathbf{M}} (\overline{\mathbf{w}}^j - \overline{\mathbf{w}}^n)\, \mathrm{d}s + \frac{1}{2} \int_0^L (\overline{\boldsymbol{\varepsilon}}^j - \overline{\boldsymbol{\varepsilon}}^n) \cdot \overline{\mathbf{K}} (\overline{\boldsymbol{\varepsilon}}^j - \overline{\boldsymbol{\varepsilon}}^n)\, \mathrm{d}s. \quad (107)$$

In the absence of applied loads, i.e. $\mathbf{f} = \mathbf{b} = \mathbf{c} = \mathbf{0}$, these results lead to the fact that the variation of the total mechanical energy of the whole multibody system in a typical time step $[t_n, t_{n+1}]$ is always smaller than the work performed by the reaction forces.

Full non-linear unconditional stability may be proved resorting to the same guidelines employed for the MP-EP scheme, i.e. ensuring that the algorithmic reaction forces perform null work within the time step for ideal, time-independent constraints. Referring to a pair of mutually constrained rigid bodies $\mathcal{B}_A$ and $\mathcal{B}_B$, we require that the averaged constraint tensors $\mathbf{A}_A^h$, $\mathbf{A}_B^h$ and $\mathbf{A}_A^g$, $\mathbf{A}_B^g$ are such that

$$\mathbf{A}_B^{h\,T} \boldsymbol{\eta}_B^j - \mathbf{A}_A^{h\,T} \boldsymbol{\eta}_A^j = \boldsymbol{\phi}^j - \boldsymbol{\phi}^n, \quad (108)$$

$$\mathbf{A}_B^{g\,T} \boldsymbol{\eta}_B^{n+1} - \mathbf{A}_A^{g\,T} \boldsymbol{\eta}_A^{n+1} = \boldsymbol{\phi}^{n+1} - \boldsymbol{\phi}^n, \quad (109)$$

since this leads to

$$\boldsymbol{\eta}_B^j \cdot \mathbf{A}_B^h \boldsymbol{\lambda}^h - \boldsymbol{\eta}_A^j \cdot \mathbf{A}_A^h \boldsymbol{\lambda}^h = 0, \quad (110)$$

$$\boldsymbol{\eta}_B^{n+1} \cdot \mathbf{A}_B^g \boldsymbol{\lambda}^g - \boldsymbol{\eta}_A^{n+1} \cdot \mathbf{A}_A^g \boldsymbol{\lambda}^g = 0, \quad (111)$$

being the left-hand sides equal to zero given that $\boldsymbol{\phi}^n = \mathbf{0}$ at the beginning of the time step. The averaged constraint matrices $\mathbf{A}_A^h$, $\mathbf{A}_B^h$ and $\mathbf{A}_A^g$, $\mathbf{A}_B^g$ can be found as shown for the MP-EP scheme, yielding equal and opposite algorithmic work over the generalized displacements $\boldsymbol{\eta}_A^j, \boldsymbol{\eta}_B^j$ and $\boldsymbol{\eta}_A^{n+1}, \boldsymbol{\eta}_B^{n+1}$. This implies the vanishing of the total reaction work for the body pair, so we can conclude by Eqs. (104) and (106) that the total mechanical energy of the system is rigorously dissipated in the absence of applied loads.

Furthermore, the identity of the 'averaged' constraint tensors $\mathbf{A}_A^h \equiv \mathbf{A}_B^h$ and $\mathbf{A}_A^g \equiv \mathbf{A}_B^g$ holds even in this case, so that we have the additional property of exact conservation for the total linear and angular momenta of the system for force-free motions.

4. Numerical applications

Some numerical examples are reported in the following to illustrate the main features of the proposed methodology. Non-linear unconditional stability and the need for high-frequency damping in

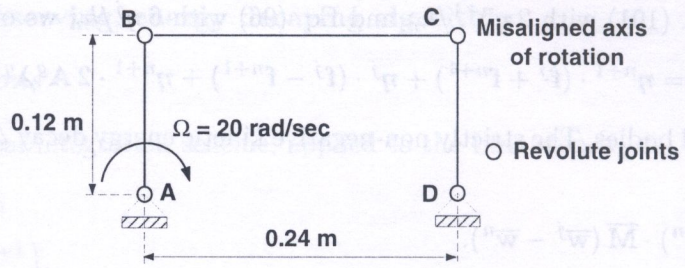

Fig. 1. The four bar mechanism problem

Table 1. Four bar mechanism: physical properties

axial stiffness	$EA_{AB} = EA_{CD} = 4.0 \cdot 10^7$ N	$EA_{BC} = 4.0 \cdot 10^7$ N
torsional stiffness	$GJ_{AB} = GJ_{CD} = 2.8 \cdot 10^4$ Nm^2	$GJ_{BC} = 2.8 \cdot 10^5$ Nm^2
bending stiffness	$EI_{AB} = EI_{CD} = 2.4 \cdot 10^4$ Nm^2	$EI_{BC} = 2.4 \cdot 10^6$ Nm^2
mass per unit span	$M_{AB} = M_{CD} = 1.6$ kg/m	$M_{BC} = 3.2$ kg/m
length	$L_{AB} = L_{CD} = 0.12$ m	$L_{BC} = 0.24$ m

non-linear multibody dynamics have been already discussed in [2–4, 7, 9, 10]. Here we limit the presentation of numerical results to the simulation of two simple flexible multibody systems.

First, we consider the four bar 'crooked' mechanism depicted in Fig. 1. The bars are modeled as geometrically exact elastic beams (except for bar AD, which represents the fixed 'ground'), linked by revolute joints at each tip. The axes of the joints at points A, B, and D are normal to the plane, while the joint axis at point C is tilted 5° from the plane normal in order to simulate an initial defect in the mechanism. The axis of the rotation that brings the plane normal into the defective joint axis is aligned with the initial direction of bar CD. The physical characteristics of the three bars are reported in Table 1. The system is driven by a constant angular velocity actuator at point A with $\Omega = 20$ rad/s. Given the defect in the joint at point C, the system undergoes a complex three-dimensional motion. The same problem was analyzed in [2, 7]. All plots refer to simulations performed with a constant time step $h = 1E - 03$ s.

The results obtained by the MP-EP and MP-ED schemes do not display any noticeable difference compared to those obtained by the EP and ED schemes, two very similar algorithms recently presented in [7]. These are based on the exponential rather than Cayley's parameterization and in general do not ensure the exact preservation of momenta. Figures 2 and 3 show the time history of the components of the linear velocity of point C and of the quarter-point internal forces for bar AB as computed by the MP-EP scheme. The same quantities as computed by the MP-ED scheme are plotted in Figs. 4 and 5. It is apparent that, in spite of its non-linear unconditional stability, the MP-EP scheme does not provide any means to remove the higher frequency content from the response. On the contrary, the MP-ED scheme is able to effectively cut off undesired oscillations while preserving the low-frequency behavior.

Second, we consider the same system without the constraint conditions on the ground at points A and D. This application is meant to provide a direct comparison between the MP-ED scheme and the analogous ED scheme recently developed in [7], showing the additional preservation capabilities of the former. In this case, we excite the free-flying mechanism by the application of three forces $\{\mathbf{n}_k\}_{k=1,2,3}$ at points B, C, and D, respectively. These forces are given by $\mathbf{n}_1 = 200\, f_0(t)\, \mathbf{i}_3$, $\mathbf{n}_2 = 400\, f_0(t)\, \mathbf{i}_1$, $\mathbf{n}_3 = -200\, f_0(t)\, \mathbf{i}_3$, where $f_0(t)$ is the triangular pulse defined as

$$f_0(t) = \begin{cases} 4\,t, & 0\text{ s} \le t < 0.025\text{ s}, \\ 2 - 4\,t, & 0.025\text{ s} \le t < 0.050\text{ s}, \\ 0, & 0.050\text{ s} \le t, \end{cases}$$

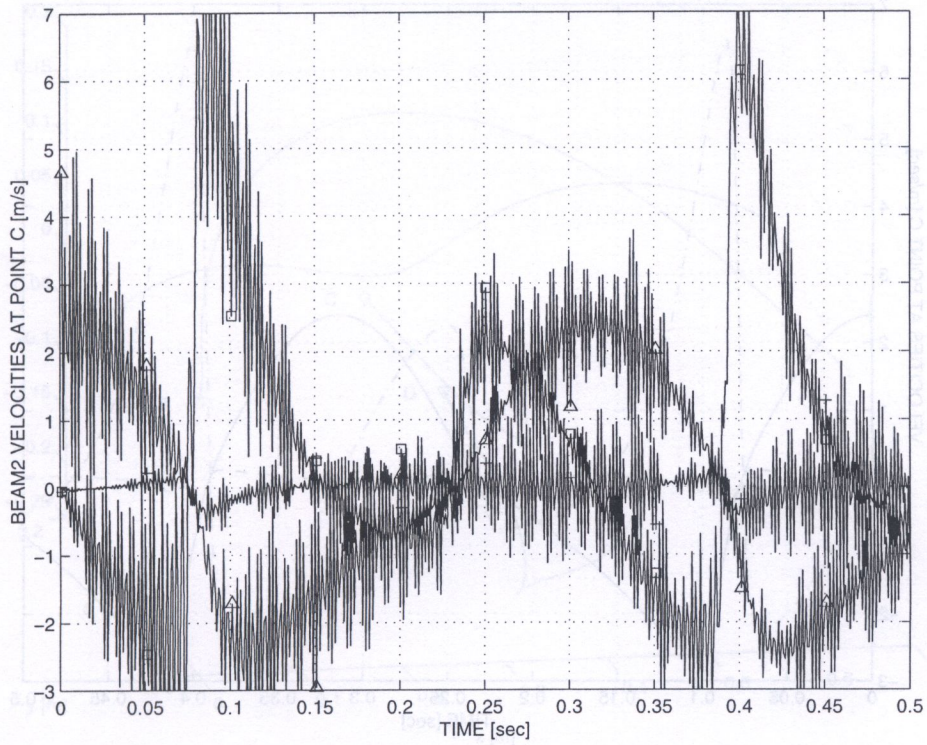

Fig. 2. Four bar mechanism: time history of velocities at point C computed with the MP-EP scheme (velocity components: $v_1 = \triangle$, $v_2 = \square$, $v_3 = +$)

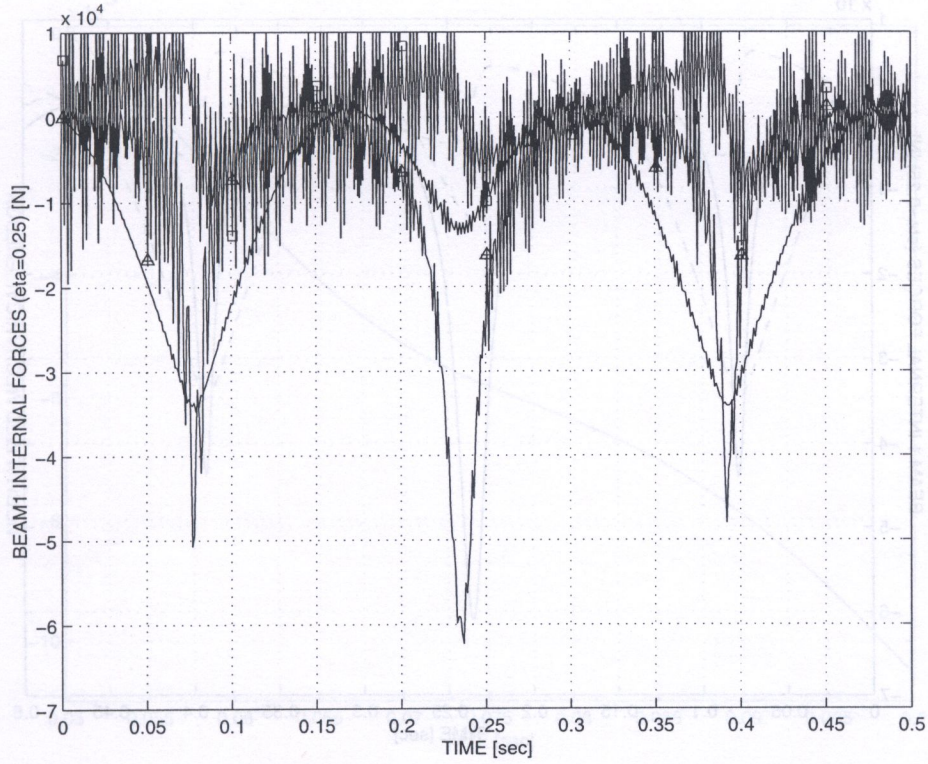

Fig. 3. Four bar mechanism: quarter-point forces in bar AB computed with the MP-EP scheme (axial force $= \triangle$, in-plane shear force $= \square$, out-of-plane shear force $= +$)

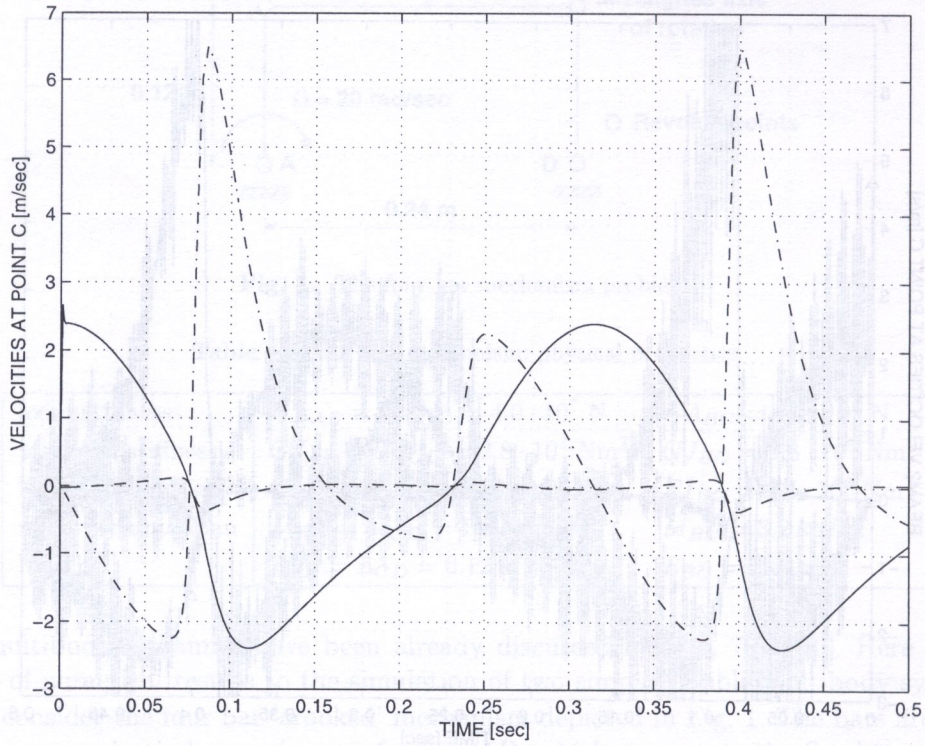

Fig. 4. Four bar mechanism: time history of velocities at point C computed with the MP-ED scheme (velocity components: v_1 = solid line, v_2 = dash-dotted line, v_3 = dashed line)

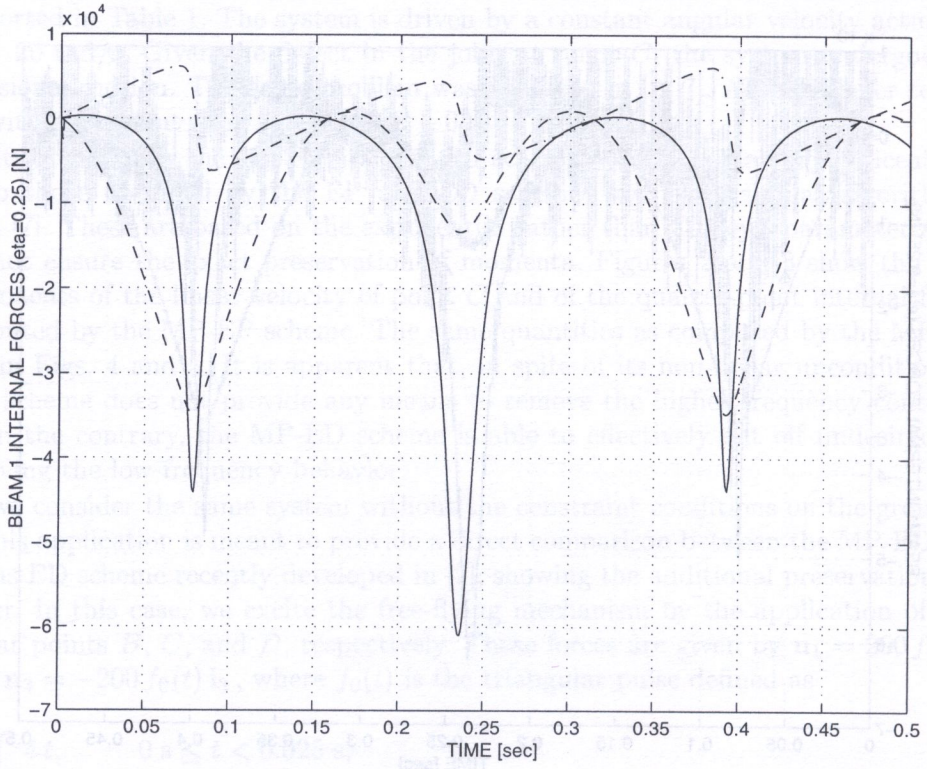

Fig. 5. Four bar mechanism: quarter-point forces in bar AB computed with the MP-ED scheme (axial force = solid line, in-plane shear force = dash-dotted line, out-of-plane shear force = dashed line)

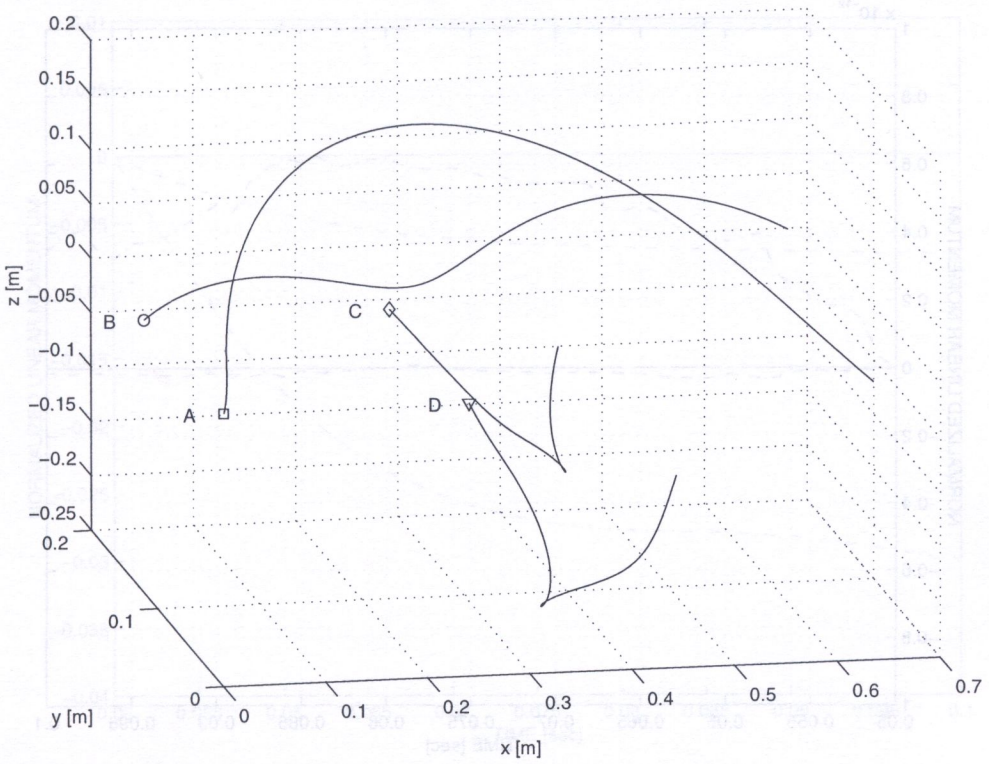

Fig. 6. Three bar free-flying mechanism: trajectories of points A, B, C, D computed with the MP-ED scheme (the symbol $\square$ marks the initial position of A, $\circ$ that of B, $\diamond$ that of C, and $\triangledown$ that of D)

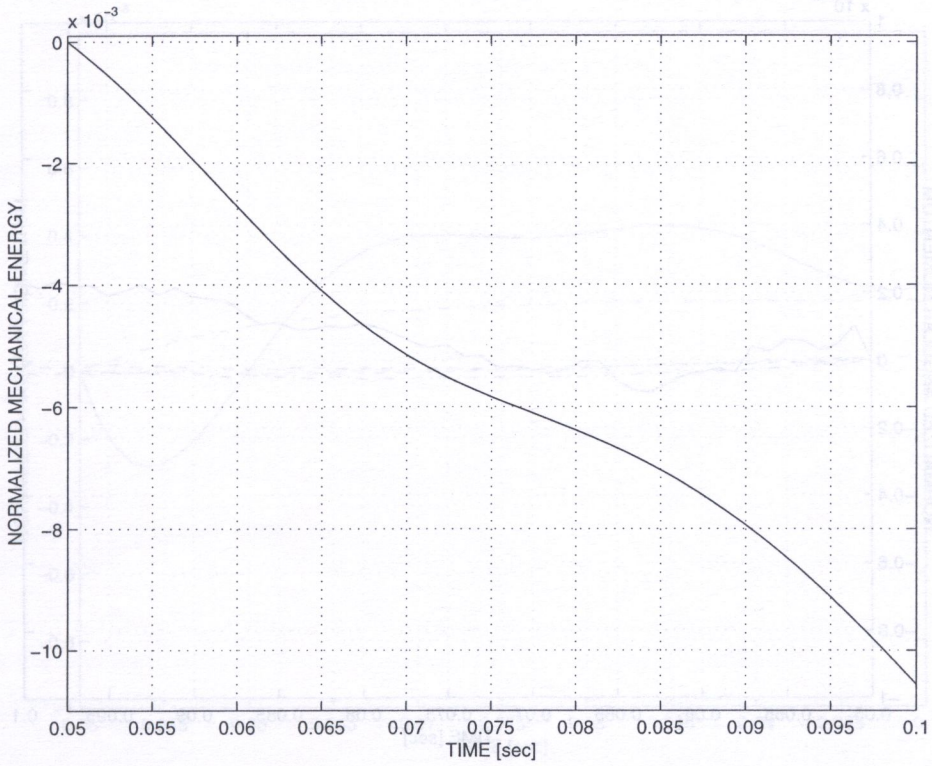

Fig. 7. Three bar free-flying mechanism: time history of the normalized total mechanical energy of the system $(E(t)/E(0.05\,\mathrm{s}) - 1)$ computed with the MP-ED scheme

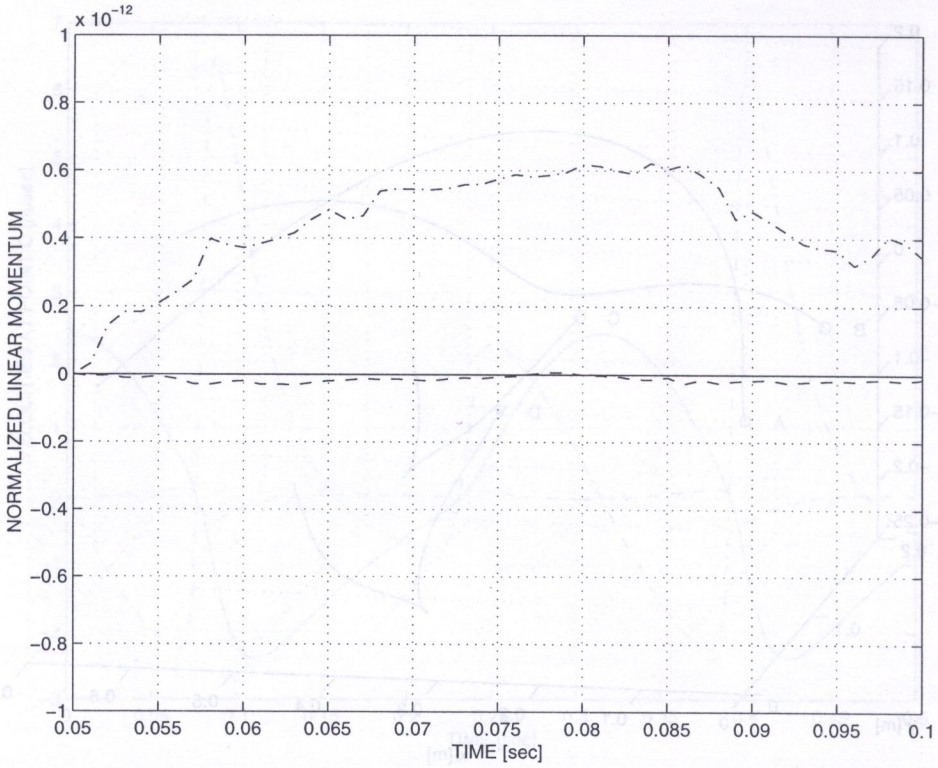

Fig. 8. Three bar free-flying mechanism: time history of the components of the normalized total linear momentum of the system $\{l_k(t)/l_k(0.05\,\mathrm{s}) - 1\}_{k=1,2,3}$ computed with the MP-ED scheme

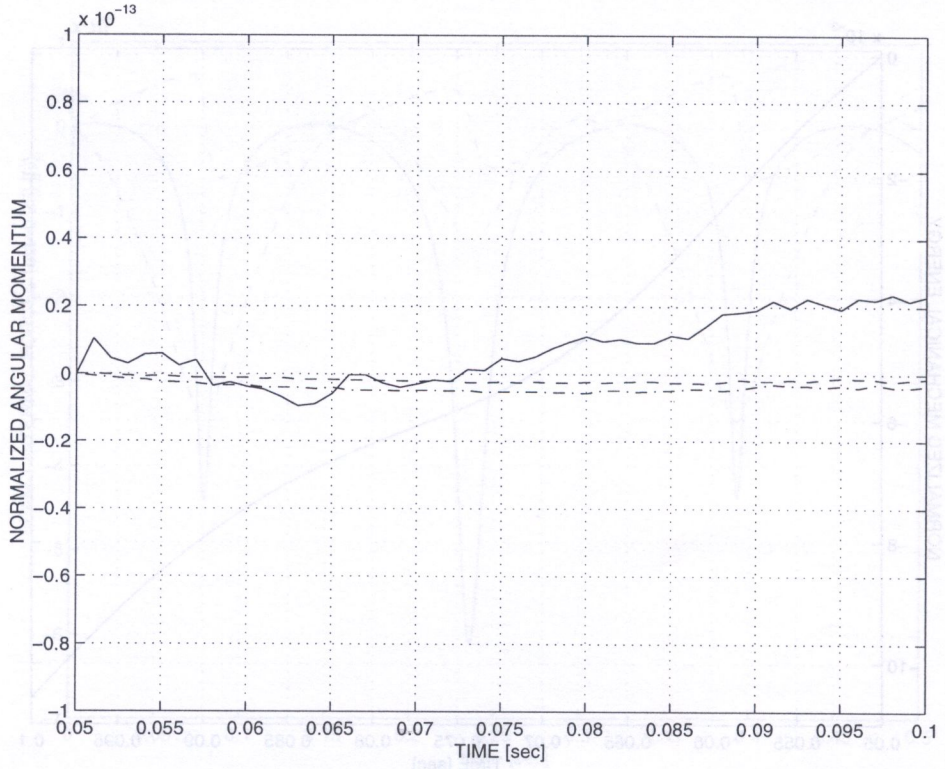

Fig. 9. Three bar free-flying mechanism: time history of the components of the normalized total angular momentum of the system $\{h_k(t)/h_k(0.05\,\mathrm{s}) - 1\}_{k=1,2,3}$ reduced to the initial position of point A, computed with the MP-ED scheme

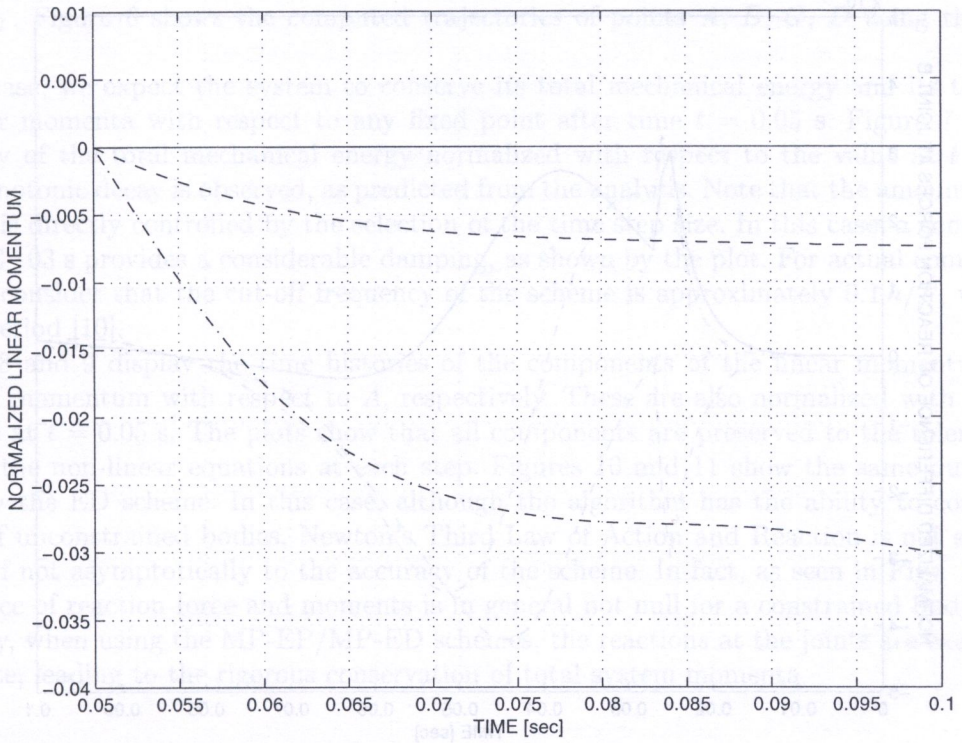

Fig. 10. Three bar free-flying mechanism: time history of the normalized total linear momentum of the system $\{(l_k(t)/l_k(0.05\,s) - 1\}_{k=1,2,3}$ computed with the ED scheme [7]

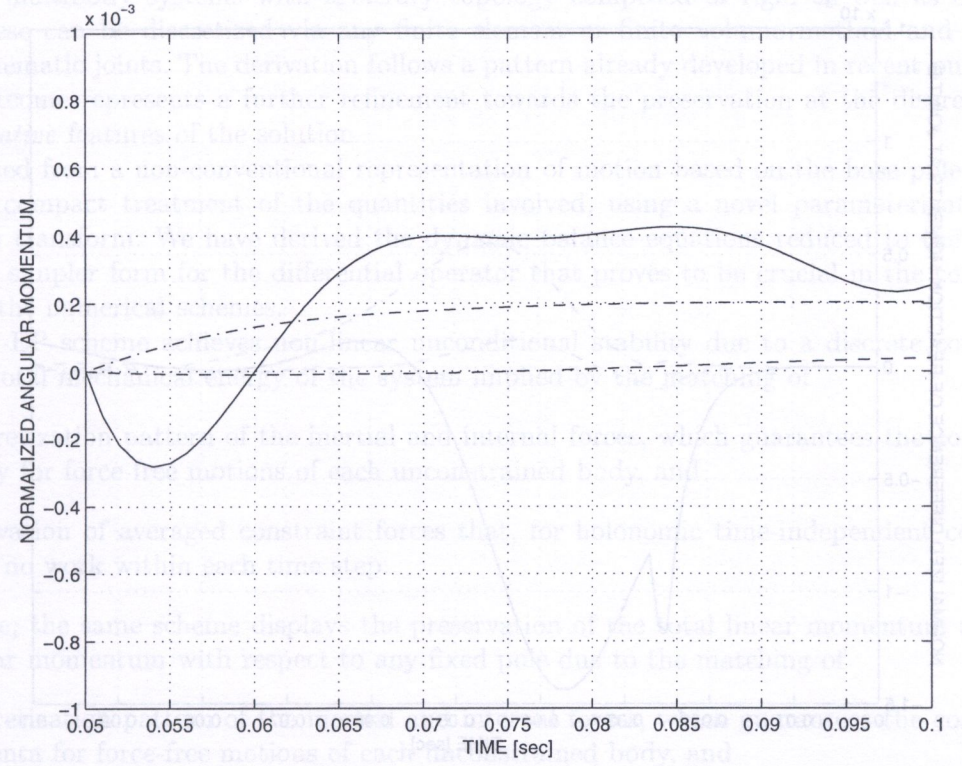

Fig. 11. Three bar free-flying mechanism: time history of the normalized total angular momentum of the system $\{(h_k(t)/h_k(0.05\,s) - 1\}_{k=1,2,3}$ reduced to the initial position of point A, computed with the ED scheme [7]

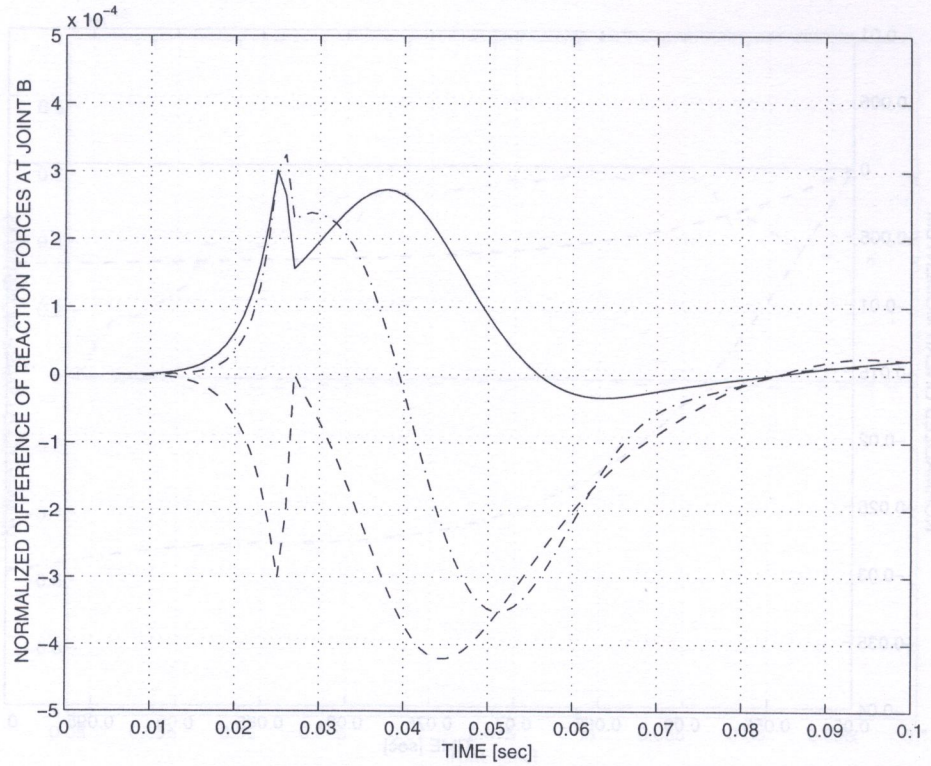

Fig. 12. Three bar free-flying mechanism: time history of the difference of the components of the reaction forces at B computed with the ED scheme [7], normalized by the respective absolute peak values in the integration time interval

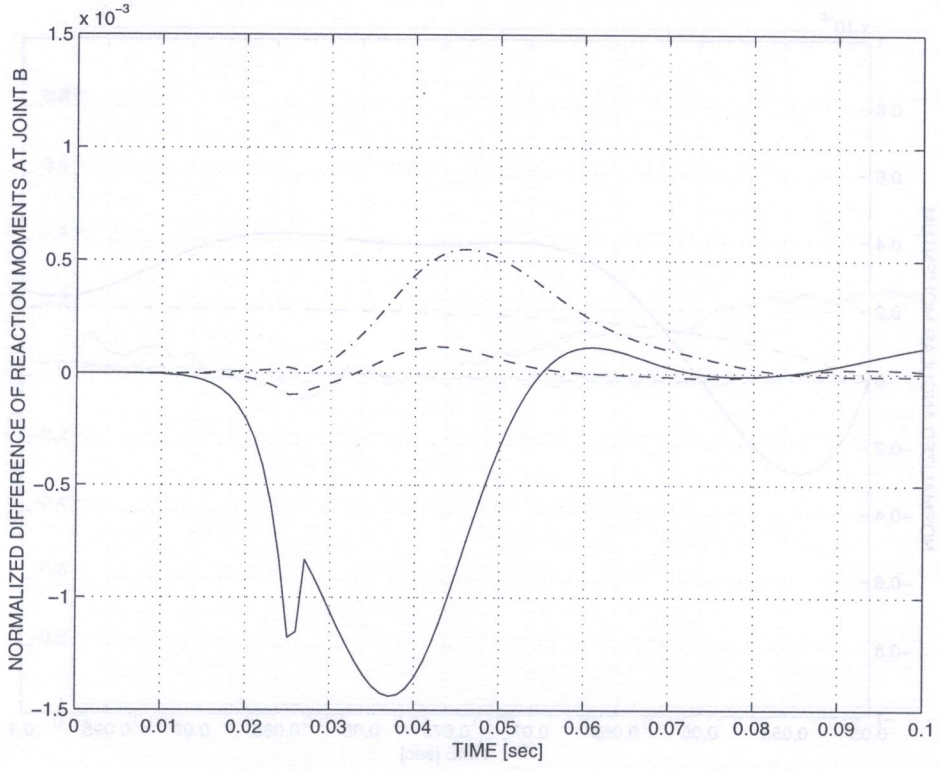

Fig. 13. Three bar free-flying mechanism: time history of the difference of the components of the reaction moments at B computed with the ED scheme [7], normalized by the respective absolute peak values in the integration time interval

and $\mathbf{i}_1$ coincides with the direction AD in the initial configuration, $\mathbf{i}_2$ with the direction AB, and $\mathbf{i}_3 = \mathbf{i}_1 \times \mathbf{i}_2$. Figure 6 shows the computed trajectories of points A, B, C, D using the MP-ED scheme.

In this case, we expect the system to conserve its total mechanical energy and its total linear and angular momenta with respect to any fixed point after time $t = 0.05$ s. Figure 7 shows the time history of the total mechanical energy normalized with respect to the value at $t = 0.05$ s. A strict monotonic decay is observed, as predicted from the analysis. Note that the amount of energy dissipation is directly controlled by the selection of the time step size. In this case, a constant time step $h = 1\text{E}{-}03$ s provides a considerable damping, as shown by the plot. For actual computations, one should consider that the cut-off frequency of the scheme is approximately $0.1\,h/T$, where T is the mode period [10].

Figures 8 and 9 display the time histories of the components of the linear momentum and of the angular momentum with respect to A, respectively. These are also normalized with respect to their values at $t = 0.05$ s. The plots show that all components are preserved to the tolerance used for solving the non-linear equations at each step. Figures 10 and 11 show the same quantities as obtained by the ED scheme. In this case, although the algorithm has the ability to conserve the momenta of unconstrained bodies, Newton's Third Law of Action and Reaction is not satisfied at the joints, if not asymptotically to the accuracy of the scheme. In fact, as seen in Figs. 12 and 13, the difference of reaction force and moments is in general not null for a constrained body pair. On the contrary, when using the MP-EP/MP-ED schemes, the reactions at the joints are exactly equal and opposite, leading to the rigorous conservation of total system momenta.

5. Conclusions

In this paper we have presented a novel methodology for the robust integration of flexible multibody system dynamics. We have designed a non-linearly unconditionally stable algorithm that allows the analysis of multibody systems with arbitrary topology composed of rigid as well as deformable bodies. These can be discretized via any finite element or finite volume method and connected through kinematic joints. The derivation follows a pattern already developed in recent publications, and the outcome represents a further refinement towards the preservation at the discrete level of some *qualitative* features of the solution.

We started from a non-conventional representation of motion based on the base pole reduction and a 6-D compact treatment of the quantities involved, using a novel parameterization based on Cayley's transform. We have derived the dynamic balance equations reduced to the base pole obtaining a simpler form for the differential operator that proves to be crucial in the conservation features of the numerical schemes.

The MP-EP scheme achieves non-linear unconditional stability due to a discrete conservation law of the total mechanical energy of the system implied by the matching of

1. the discretization pattern of the inertial and internal forces, which guarantees the conservation of energy for force-free motions of each unconstrained body, and

2. the derivation of averaged constraint forces that, for holonomic time-independent constraints, perform no work within each time step.

Furthermore, the same scheme displays the preservation of the total linear momentum and of the total angular momentum with respect to any fixed pole due to the matching of

1. the discretization pattern of the inertial and internal forces, which guarantees the conservation of momenta for force-free motions of each unconstrained body, and

2. the use of Cayley's parameterization, which entails averaged constraint reaction forces equal in magnitude and direction and opposite in sign for each constrained body pair.

We remark that, although not directly connected to stability enhancement, the preservation of momenta is indeed a considerable feature, achieved at no additional cost.

The MP-ED scheme retains all of these features, but for the substitution of the discrete energy conservation law with a statement of strict decay of the total mechanical energy of the system, at the cost of the introduction of an additional internal stage. As a result, the scheme displays an enhanced robustness related to its capacity of damping out the unresolved high frequencies. The method has been tested with the help of numerical examples, confirming the predicted properties of the methodology.

REFERENCES

[1] O.A. Bauchau, C.L. Bottasso, L. Trainelli. Robust integration schemes for flexible multibody systems, *Comp. Meth. Appl. Mech. Engrg.*, to appear.

[2] O.A. Bauchau, C.L. Bottasso. On the design of energy preserving and decaying schemes for flexible non-linear multi-body systems, *Int. J. Num. Meth. Engrg.*, **38**: 2727–2751, 1995.

[3] O.A. Bauchau, N.J. Theron. Energy decaying scheme for nonlinear beam models, *Comp. Meth. Appl. Mech. Engrg.*, **134**: 37–56, 1996.

[4] O.A. Bauchau, N.J. Theron. Energy decaying scheme for nonlinear elastic multibody systems, *Comput. & Struct.*, **59**: 317–331, 1996.

[5] M. Borri, L. Trainelli, C.L. Bottasso. On the representation and parameterization of motion, *Multibody System Dynamics*, **4**: 129–193, 2000.

[6] M. Borri, C.L. Bottasso, L. Trainelli. Integration of elastic multibody systems by invariant conserving/dissipating algorithms – Part I: Formulation, *Comp. Meth. Appl. Mech. Engrg.*, **190**: 3669–3699, 2001.

[7] C.L. Bottasso , M. Borri, L. Trainelli. Integration of elastic multibody systems by invariant conserving/dissipating algorithms – Part II: Numerical schemes and applications, *Comp. Meth. Appl. Mech. Engrg.*, **190**: 3701–3733, 2001.

[8] M. Borri, C.L. Bottasso, L. Trainelli. Geometric invariance, submitted to *Comp. Mech.*

[9] C.L. Bottasso, M. Borri. Integrating finite rotations, *Comp. Meth. Appl. Mech. Engrg.*, **164**: 307–331, 1998.

[10] C.L. Bottasso, M. Borri. Energy preserving/decaying schemes for non-linear beam dynamics using the helicoidal approximation, *Comp. Meth. Appl. Mech. Engrg.*, **143**: 393–415, 1997.

[11] C.L. Bottasso, A new look at finite elements in time – A variational interpretation of Runge–Kutta methods, *Appl. Num. Math.*, **25**: 355–368, 1997.

[12] J.C. Simo, N. Tarnow, M. Doblare. Non–linear dynamics of three–dimensional rods: exact energy and momentum conserving algorithms, *Int. J. Num. Meth. Engrg.*, **38**: 1431–1473, 1995.

[13] J.C. Simo, N. Tarnow. The discrete energy–momentum method. Conserving algorithms for nonlinear dynamics, *ZAMP*, **43**: 757–792, 1992.

[14] J.C. Simo, L. Vu-Quoc. On the dynamics in space of rods undergoing large motions – a geometrically exact approach, *Comp. Meth. Appl. Mech. Engrg.*, **66**: 125–161, 1988.